Investigation Into the Improved Dispersion of Nickel Oxide Over the Surface of SOFC Tubular Anodes

by

Scott Taylor

A thesis submitted to

The University of Birmingham

for the degree of

MRes.

Department of Chemical Engineering

College of Engineering

The University of Birmingham

October 2009

Acknowledgments

I would like to thank Prof. Stuart Blackburn for his help and support during this project after a very awkward start, as well as the members of the Ceramics Forming Group, Interdisciplinary Research Centre who offered help with both equipment and expertise during this project. I would also like to thank the E.P.S.R.C for the funding which enabled me to carry out this project and Dr. Richard Greenwood for his advice.

Abstract

Issues with nickel agglomeration and reduced porosity of SOFC anode tubes have been noted in previous investigations using carbon black as a porosity forming agent, this thesis looks at methods of improving these issues by investigation of alternative materials (carbon, graphite, flour) along with alternative processing methods. The porosity forming agent of the SOFC anode was investigated to establish the most effective material to improve nickel dispersion. The effect of powder processing by milling to improve mixing and particle size distribution within the anode mixture before extrusion and sintering was also investigated.

Powder processing by means of milling was seen to offer significant improvements in dispersion of nickel over the surface of tubes, along with a distinct improvement in the porosity of the sintered tubes. Of the three porosity forming agents investigated wheat flour offered the best solution to the issues of nickel dispersion and increasing tube porosity, it was also found to be the easiest material to process and form into tubes.

Table of contents

List of figures

List of tables

1. INTRODUCTION

Solid Oxide Fuel Cells (SOFCs) are electrochemical conversion devices that directly oxidise fuel to produce electricity, a good analogy is to think of them as a large battery but rather than completely depleting its fuel source fuel is constantly passed through it. SOFCs have many advantages over other energy production methods, they run with a high efficiency typically around 60% which can be increased by using waste gasses to run turbines[1], they also have the flexibility to work with various fuel sources unlike Proton Exchange Membrane Fuel Cells (PEMFCs) whose catalysts can be poisoned by certain gasses.

SOFCs operate by fuel passing over an anode, and air passing over the cathode. At the anode oxidation of the fuel takes place which releases an electron and consequently an electric charge. At the same time reduction of the air takes place at the cathode which receives the free electron which has been released from the anode after passing through the electrolyte. The resultant electric charge is captured, with the only waste products being water, air and excess fuel which can be re-used, however there is only a very small charge released due to oxidation of the fuel.[2] This small charge combined with the relatively small size of the tube mean that it is important to have as many three phase boundaries or triple boundary points (TBPs) where these reactions take place per unit area as possible. Fig.1[2]. shows a typical TBP where the reactive nickel, the Yttria Stabilised Zirconia (YSZ) and the gaseous fuel and oxygen meet.

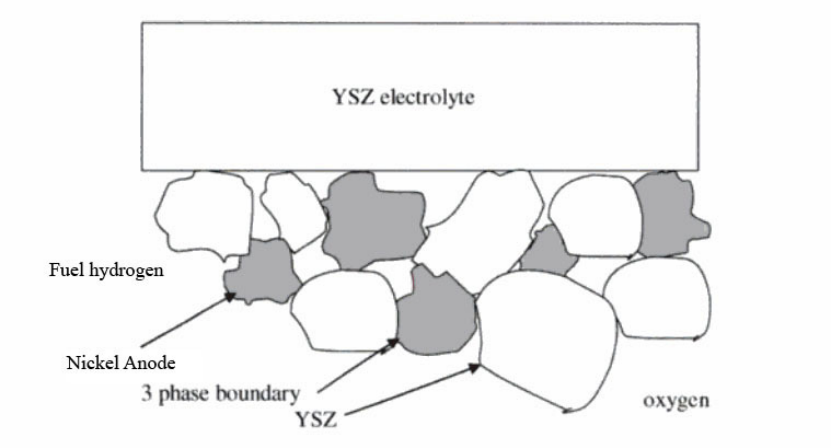

Fig.1. Triple boundary point within SOFC anode[2]

1.1. Aim

The aim of this investigation is to address an issue of nickel oxide agglomeration and decreased tube porosity in previous studies at the University of Birmingham and to improve the dispersion of nickel over the surface of the SOFC anode along with improving the porosity of the anode. By doing this the number of TBPs will be increased and the efficiency of any SOFC tubes produced in the future should be increased.

1.2. Thesis layout

Within this thesis, the literature review, chapter 2, outlines the background, operation and construction of SOFCs along with methods of powder processing. The main experimental section, chapter 3, contains all experimental work, materials, methodologies and results. Starting with initial experiments and following experimental stages in the order they were carried out during this investigation, finishing with the final SEM analysis, for each section methods, discussions and results are given. The final sections draw together conclusions from the experimental section, chapter 4, and chapter 5 proposes future work.

2. LITERATURE REVIEW

2.1. Solid oxide fuel cells

2.1.1. Background

Solid oxide fuel cells (SOFCs) are currently the most efficient devices available for the direct conversion of chemical fuels into electrical power. The basic idea and materials behind an SOFC were proposed in the mid 1890's by Nernst[3] in the form of a lamp with a thin Zirconium rod taking place of the carbon filament found in regular lamps of the time.

Due to the failure of Nernst's lamp to compete with regular lamps of the period there was very little development of SOFCs until the late 1930's when Baur and Preis[4] demonstrated the first fuel cell stack and speculated that the SOFC stack would be able to compete with batteries as a viable power source.

Development of SOFCs was slow until the 1970s when Westinghouse Electric Corporation developed a tubular SOFC design which led to the first 5kW SOFC generator[5]. During the 1980s and 1990s the manufacturing techniques available meant that the manufacture of planar cells was more economical than that of tubular cells and so the majority of research and development focused on the planar cell layout[6]. Some focus is now turning back towards tubular fuel SOFCs in particular micro tubular cells suitable for rapid start up for uses within vehicles.[2]

Solid oxide fuel cells operate as an electrochemical conversion device and can be thought of as batteries which have a constant fuel supply rather than a finite amount. They operate at temperatures typically between 600-1000°C, where the solid oxide electrolyte made from ceramic such as Yttria stabilised Zirconia (YSZ) acts as a conductor of oxide ions. Oxygen atoms found in air are reduced on the porous cathode by electrons, thus being

converted into ions, these ions pass through the solid electrolyte to the fuel rich porous anode where the ions interact with hydrogen (in this case) causing oxidation and giving up electrons to an external circuit, this can be seen in Fig.2.[7]

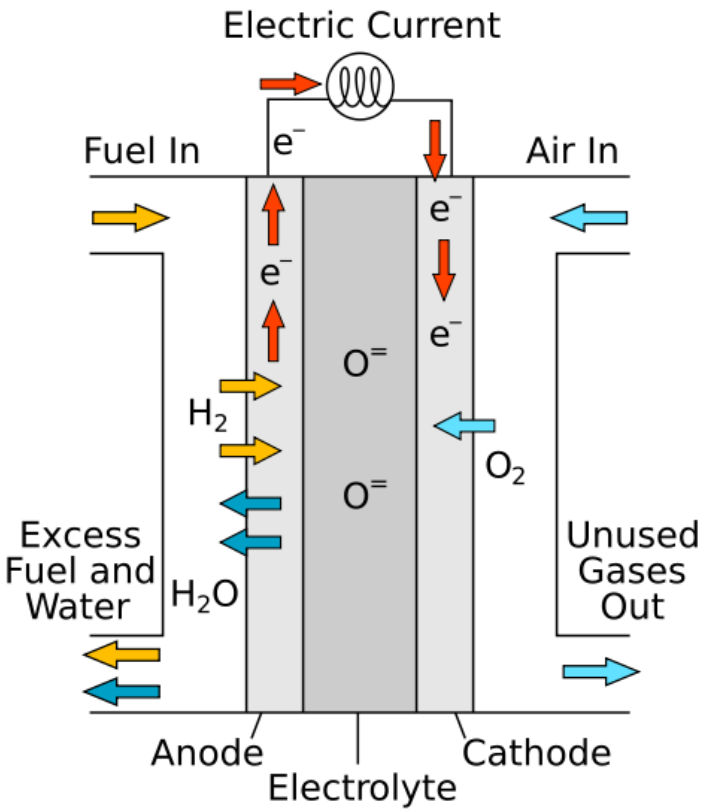

Fig.2. Schematic of SOFC operation[7]

2.1.2. Construction and materials

SOFCs can be formed in several configurations and by various production methods. In the late 1970s electrochemical vapour deposition began to be used to produce tubular cells of around 15-20 mm in diameter. Zirconium chloride plus yttrium chloride vapour was passed along the outside of a porous tube of the cathode material whilst water vapour was passed along the inside of the tube. This lead to the deposition of a Yttria doped zirconium layer being formed over the surface of the tube.[8]

Tape casting is another method of production and involves the formation of a slurry or paste of anode, cathode and electrolyte materials respectively. These pastes are then tape cast, or layered onto each other and left to dry before sintering to form an SOFC. This method of production is suitable for the manufacture of planar SOFCs rather than tubular SOFCs.[9]

Extrusion involves the formation of pastes similar to those used within tape casting however; they are extruded through a die in a press to form a tubular SOFC. Layers of other materials are then tape cast or screen printed onto the surface of this tube to form a tubular structure with several layers instead of being layered on top of each other to form a flat planar cell.

Planar SOFCs are made up of a set of flat plates which are connected in electrical series, the basic structure and components of a planar SOFC can be seen in Fig.3.[10]. As mentioned above planar SOFCs can be produced using several different methods which allows them to be made into various structures as well as being relatively economic to manufacture.[11]

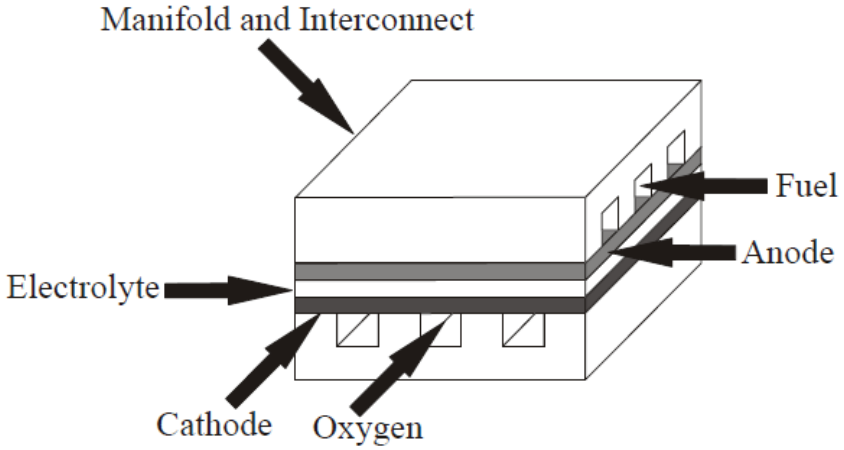

Fig.3. Operation of a planar SOFC[10]

Whilst planar SOFCs have the advantage of being relatively cheap to produce, and due to the nature of their construction can be stacked to form dense arrays with higher power densities, they suffer from thermal stresses generated by thermal cycling experienced during operation.[12] To overcome this and to prolong life spans start up times are longer when compared to tubular SOFCs.

Tubular SOFCs as the name suggests are constructed in a tubular arrangement, most commonly they follow a fuel cell design developed by Westinghouse Electric Corporation, the design of which can be seen in Fig.4.[13]. Tubular SOFCs are generally manufactured by the extrusion process with methods such as electrochemical vapour deposition being used to add extra layers.

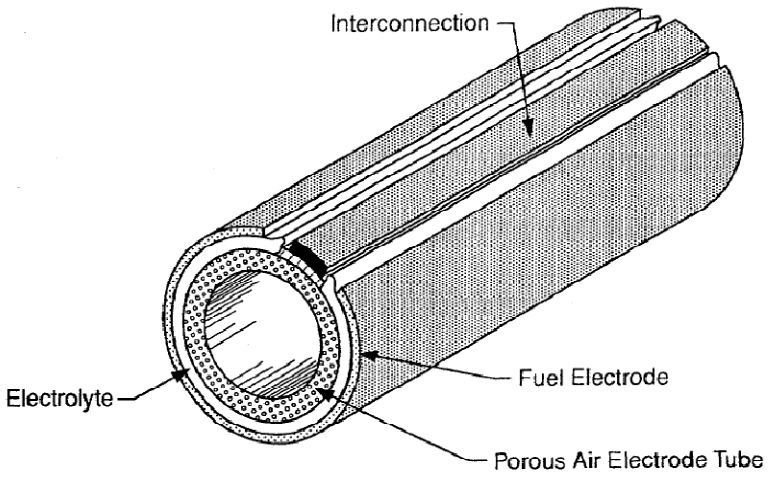

Fig.4. Schematic of a tubular SOFC[13]

Whilst planar SOFCs suffer from thermal stresses and issues with thermal cycling, tubular SOFCs are far more physically resistant and far less likely to crack. However due to the cell design being tubular and having a lower packing density than a planar cell tubular SOFC stacks have a lower power density than planar stacks.

Tubular SOFCs are relatively simple devices in construction, as can be seen in Fig.4. there are only 5 components required to construct a cell, those being:

Electrolyte Typically non porous Yttrium Stabilised Zirconium (YSZ)

Anode Typically a porous YSZ Nickel cermet.

Cathode Typically porous Lanthanum manganite based.

Two interconnect wires Typically Rare earth Chromite alloy wires.

2.1.3. Anode composition

An anode must be catalytically active for fuel oxidisation to take place, as well as being electrically conductive to allow the flow of ions to an external circuit. Along with these two properties it must have a very porous body to allow for the flow or fuel and air through it to allow the oxidation reactions to take place.

Many materials have been investigated to establish their suitability; precious metals such as gold and platinum were used early on in the development by Haber in 1905 when still at low operating temperatures.[14] Möbius selected platinum along with other transition metals, due to its high temperature stability and catalytic properties[15]. However platinum was seen to be unsuitable due to the fact it does not bond well to the electrolyte and tends to fail in service, spalling off, probably due to the electrochemical generation of water at the interface.[16]

Nickel had been investigated and had been seen to operate well, however nickel suffers from grain growth and agglomeration at high temperatures which has a detrimental effect on the anodes ability to carry out oxidisation of the fuel due to lack of porosity. It is also known that nickel has a significant thermal expansion difference to that of YSZ, due to

these problems the adoption of an all metal anode has not found acceptance in SOFC technology. It was first noted by Spacil that these problems could be overcome by the mixing of YSZ particles with the nickel to form a composite anode structure. [17]

2.1.4. Anode porosity

NiO YSZ cermets are the most commonly used materials in the manufacture of SOFC anodes, many studies since the first by Spacil in 1964 have shown this to be a good method of production. Studies by Kim *et al*[18], Yang *et al*[19], Martins *et al*[20] etc. have all investigated using a NiO YSZ cermet with varying levels of success. To form the porosity required within the anode after sintering NiO is reduced under hydrogen, this reduction of the nickel oxide to the metal leads to a 25% reduction in the nickel volume leading to the desired porosity[16].

An alternative method to improve the porosity and to improve the distribution of pores is to use a porosity agent, that is a sacrificial material that will be burnt off during the sintering process leaving behind pores. Studies by Yu *et al*[21] have shown that carbon can be successfully used as a porosity agent, carbon black was used by Powell[22] which raised issues with nickel growth and agglomeration possibly enhanced by the lack of an even pore distribution.

As the porosity agent is simply burnt off during the sintering process any material which combusts below the sintering temperature of the NiO YSZ cermet can be used for this task providing that it is clean burning. Investigations by Ai *et al*[23] have shown that regular wheat flour can be used successfully as a porosity agent, the report does not however mention whether processing of the flour was required before use or if it was used as received.

2.2. Powder processing

Prior to mixing, forming into a paste and sintering, powders can be processed to alter the physical properties of the constituent powders to refine particle sizes, and to create a more uniform particles size. This is generally carried out by ball milling and mechanical alloying of the powders.

Mechanical alloying is a form of dry high energy ball milling mainly used within industry for the production of composite metal powders with a controlled fine microstructure. It is carried out with high agitated ball charge which causes repeated cold welding and fracturing of metal powders to which non metallic powders can be added. The impact force experienced is directly proportional to the mass of the medium used within the ball mill; larger balls will produce more force and be used for larger rougher particles, whereas smaller media should be used for finer powders[24].

The stages involved in the mechanical alloying process are micro forging or cold welding, fracture and finally agglomeration. There are additives which can be added to the powders to prevent agglomeration and cold welding of the powders however, the cold welding stage of the alloying process is the main interest for this project and thus these additives will not be used[25].

Fig.5. Mechanical alloying in Middle Ages [26]

Mechanical alloying is usually carried out using high energy ball milling, with processing times of around 24 hours. There are several other methods of milling available, however both attrition and disc milling having being investigated in the context of SOFC manufacture.

Mechanical alloying offers advantages to untreated powders in the form of increased sinterability of the composite material. This is due to the fact that it significantly improves the number of metal/metal contacts as opposed to metal/ceramic contacts experienced in mixed powders, this is preferential as metal/metal contacts are more reactive during sintering thus leading to a lower sintering temperature being required when compared to a non alloyed powder[25].

It is also suggested by Artz and Shultz[27] that mechanical alloying increases the strength of the resultant sintered material due to the uniform distribution of the ceramic particles along with their fine grain size. This combined with the work hardening of the metal particles within the composite leads to an increase in strength.

As noted by Kubarsepp[28] ball milling is used for the production of ceramic/metallic powders with a uniform dispersion which is widely used for the manufacture of cermets. This suggests that the technique would lend itself well to YSZ Ni powders, however NiO powder is used within the manufacturing process of the SOFC which may lead to issues due to elastic properties which do not lend themselves towards mechanical alloying..

A main issue in the production of an SOFC anode using nickel is propagation of nickel particle size due to grain growth of the nickel during the sintering process which leads to a decrease in porosity and thus a decrease in TBP's. As suggested by Kubarsepp mechanical alloying of particles can decrease the required sintering temperature of the resultant material, which should lead to a decreased nickel grain growth after sintering is completed.

Studies by Lee *et al.*[29] and Hong *et al.*[30] have shown that ball milling of SOFC cermet powders leads to more conductive composite materials after sintering, suggesting that improvements in efficiencies of SOFC's may be brought about by the use of milling. Restivo *et al.*[31] showed that mechanical alloying leads to particle refinement and high deformation of metallic constituents leading to homogeneous powders, pellets formed form these powders can then be sintered at a lower temperature than previously. This may possibly lead to a decrease in nickel grain growth, however, none of the studies look into the added cost of milling and whether the increased efficiency or decreased sintering temperature makes the mechanical alloying economically viable.

2.3. Co-extrusion

Extrusion is the process of pushing or drawing a material through a die to form it into a desired geometry. Extrusion can be carried out in various ways, by squeezing, a paste between two approaching surfaces, by feeding paste into a screw extruder, or by placing batches of pastes into a cylinder or barrel and pressing using a driven ram[32]. For the purpose of this investigation the third method using barrel and ram system will be used.

SOFC electrolyte tubes are commonly manufactured using the extrusion process, where a central substrate layer is extruded, with subsequent layers being added afterwards via processes such as screen printing or electrochemical vapour deposition a method employed by Westinghouse Electric Corporation[13]. An alternative method to this is co-extrusion in which more than one material at one time is extruded allowing all of the materials to be formed into the final structure in one process.

There are two main methods which are employed to extrude multiple pastes together, firstly the "rock candy"[33] method as used in the product of rock candy sweets, where the pastes are layered together within the barrel before extrusion through a die. When extruded

through the die they proceed to form a structure the same as within the barrel but on a finer scale. The other method is multi-billet extrusion where pastes begin in separate barrels, then extruded through a complex die and manifold system to form a single structure[22].

The rock candy method is a more simple solution for co-extrusion, however, due to the time taken preparing the preform for extrusion is a very labour intensive process and is subject to variance due to operator input[34]. This process simplicity, along with the limited time for this project and the high cost incurred by the design and manufacture of a multi-billet extrusion system meant that the rock candy method was employed in this project.

During the co-extrusion process the unification of paste rheologies is of interest as shown by Chen *at al*. during the extrusion of ZrO2 and stainless steel[35]. This is of less interest depending upon the method of paste preparation used, with some such as twin roll milling leading pastes with similar rheologies due to the self limiting mechanism of this mixing process[22].

The rock candy method extrudes several pastes as one mass, through a die which then leads to a structure composed of pastes in the same arrangement as previously however on a smaller scale, this can be seen illustrated in Fig.6.[22] Tubular structures can also be extruded using this process as shown by Van Hot *et al*[36] .To do this a solid layer of sacrificial material or "feed rod" with the layers of paste arranged around it is extruded. Within an SOFC this feed rod would be made of paste containing the sacrificial PFA so that during sintering it would pyrolise leaving the tubular structure required.

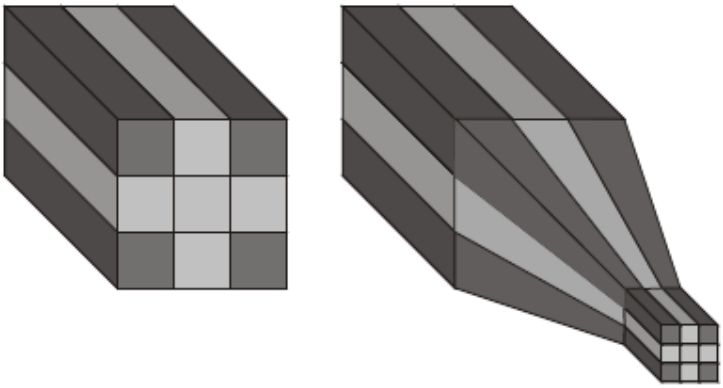

Fig.6. Showing reduction in scale after co-extrusion through die[22]

An alternative to this feed rod was employed during this investigation. That is to use a modified extruder ram with a mandrel attached centrally with the required diameter of the resultant tube. The material to be extruded is then layered around this central mandrel and as the mandrel moves slower than the extruded pastes an extruded tube will form from the end of the mandrel.

2.4. Paste rheologies

A paste is a mixture of a solid and a liquid phase[32], there is sometimes a third gas phase present such as air bubbles trapped within the paste however measures are taken to remove these before processing. It is possible to think of pastes as a one phase system, however the characterisation method used within this investigation looks at them as a two phase system considering both the solid and liquid properties.

Benbow & Bridgwater developed a four parameter model for the characterisation of pastes seen in Eqn.1[32]:

$$P = 2\ln\left(\frac{D_o}{D}\right)(\sigma_o + \alpha V) + \frac{4L}{D}(\tau_o + \beta V) \quad \text{Eqn.1}$$

Where:

P – Pressure MPa

D_o / D – Diameter of barrel m / Diameter of die m

L / D – Length of die m / Diameter of die m

V – Velocity of extrudate ms^{-1}

The four paste parameters being[32,37]:

σ_o - Bulk yield stress MPa

α - Die entry velocity factor $Pasm^{-1}$

τ_o - Die wall initial yield stress MPa

β - Die wall shear stress velocity factor $Pasm^{-1}$

Results of pressure vs velocity are plotted graphically to allow the results to be extrapolated back to zero, and to find the above parameters. If the plot of pressure vs. extrudate velocity is not linear then the four parameter model is not suitable, and the six parameter model needs to be applied as shown in Eqn.2[32].

$$P = 2\ln\left(\frac{D_o}{D}\right)(\sigma_o + \alpha V^m) + \frac{4L}{D}(\tau_o + \beta V^n) \quad \text{Eqn.2}$$

The two extra paste parameters being[32,37]:

m – Die entry velocity index

n – Die wall velocity index

3. EXPERIMENTAL PROGRAMME

3.1. Raw materials

Within this investigation several materials were used, NiO and YSZ as the main components of the SOFC anode, along with graphite, carbon black, potato starch and wheat flour investigated as porosity agents. Before processing into pastes and sintering the particle size of the individual materials was established using two methods, laser diffraction and by scanning electron microscopy (SEM). The materials used were as follows

YSZ – 8 Mol. Yttria Stabilised Zirconia HSY8 ordered from Daiichi Kigenso Kagaku Kogyo Co. Specified as 0.5μm – 0.7μm particle size.

Nio – Nickel oxide powder 325 mesh, supplied by Cerac international, unspecified particle size.

Carbon – Carbon black, Monarch 120, unspecified particle size.

Graphite – Graphite powder, unknown particle size.

Potato starch – Unknown particle size.

Wheat flour – McDougalls plain flour, made from 100% wheat gluten, unknown particle size.

3.1.1. Laser diffraction

Laser diffraction operates by passing laser light through a powder sample which is dispersed within a suitable medium, when the laser light contacts the particles of the sample it is then scattered. The scattered light is focused via a lens onto a detector, the

intensity and angle of the diffracted light is de-convoluted using a mathematical model and the particle size established.

3.1.2. Method

Laser diffraction was carried out using a Coulter SVM LS230 laser diffraction machine, all analysis was carried out using the small bath attachment, and using Polarization Intensity Differential Scattering (PIDS) which increases accuracy of the results and allows for size detection down to 0.04 μm. To keep the samples in suspension during analysis the LS230 has an internal pump. The pump speed which moves the liquid within the bath stopping sedimentation taking place was set at 40% a level sufficient to keep particles in suspension whilst not effecting results, problems with sedimentation of a sample could be improved by increasing pump speed.

Initially the suspension medium for the samples needed to be established, to this end small amounts of each material were placed into small glass vials, water was added and the vials were agitated by hand shaking for approximately one minute. They were then left for three minutes to observe the sedimentation behaviour.

Any materials that did not suspend were tested in a 50/50 volume mixture of water and glycerol, and if they still did not suspend then roughly 1:100 volume Dispex a40 (a narrow-fraction ammonium salt, acrylic dispersant supplied by Ciba) water solution was used. All materials other than YSZ were suspended in either water or a water glycerol mix.

The YSZ powder proved to be the most difficult material to establish the particle size, firstly it was very difficult to suspend, sedimenting quickly in both water and water glycerol mixes due to its relatively high density, it remained in suspension for over 2 minutes within a water Dispex solution and was tested in this form. The Fraunhofer optical

model was applied and a mean average particle size of 65µm by volume was returned. This was very high as the powder was specified to be between 0.5 and 0.7µm in size. This discrepancy in the particle size suggested that a large amount of agglomeration had taken place. To overcome this, the YSZ was placed in a 1% solution of dispex and left in an ultrasonic bath for 15 minutes, this left it well dispersed and in a good suspension ready for analysis to be undertaken, the results of which can be seen in section 3.1.3.

3.1.3. Results

After carrying out laser diffraction runs on the various particles the following particle size distributions were found. All graphs show volume percentage of particles within samples.

Fig.7. shows the particle size distribution for the YSZ powder after suspension in Dispex and excitation within an ultrasonic bath. A large peak is seen at 0.6 µm which is to be expected as this was the specified particle size from the suppliers. There is however another peak at around 3 µm suggesting there is still some agglomeration of particles occurring. Laser diffraction showed the powder to have an average size of 0.627 µm.

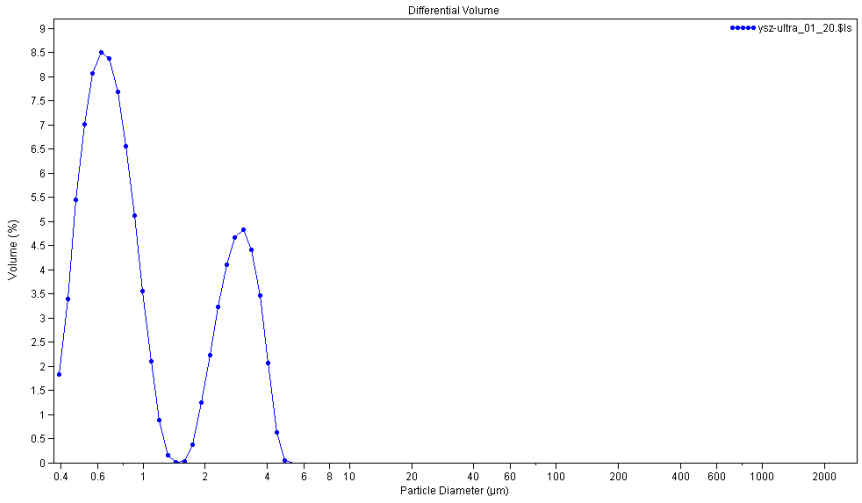

Fig.7. YSZ powder particle size distribution.

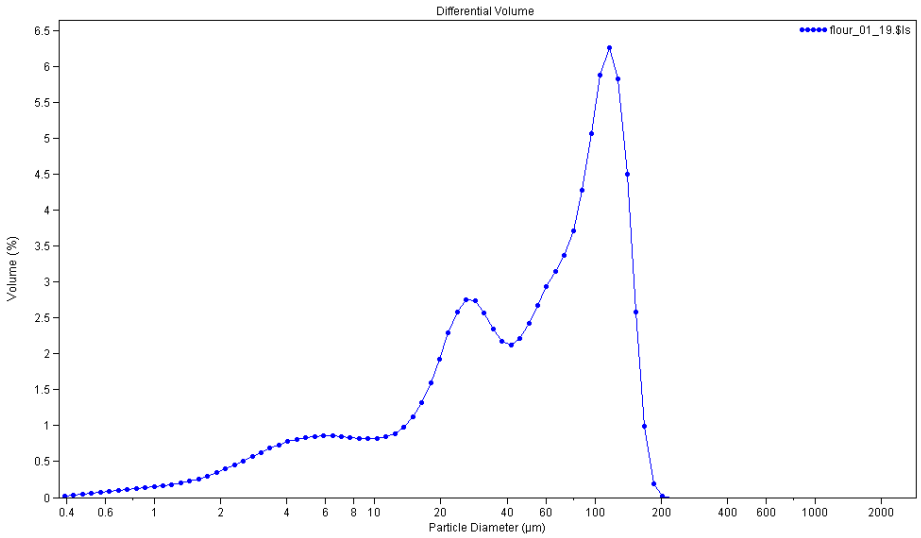

Fig.8. Wheat flour particle size distribution.

Fig.8. Shows the particle size distribution for the wheat flour, the powder was seen to be quite coarse having an average particle size of 63.2 µm, along with a large spread in size distribution. This would be expected as it is not milled to a uniform size during its production.

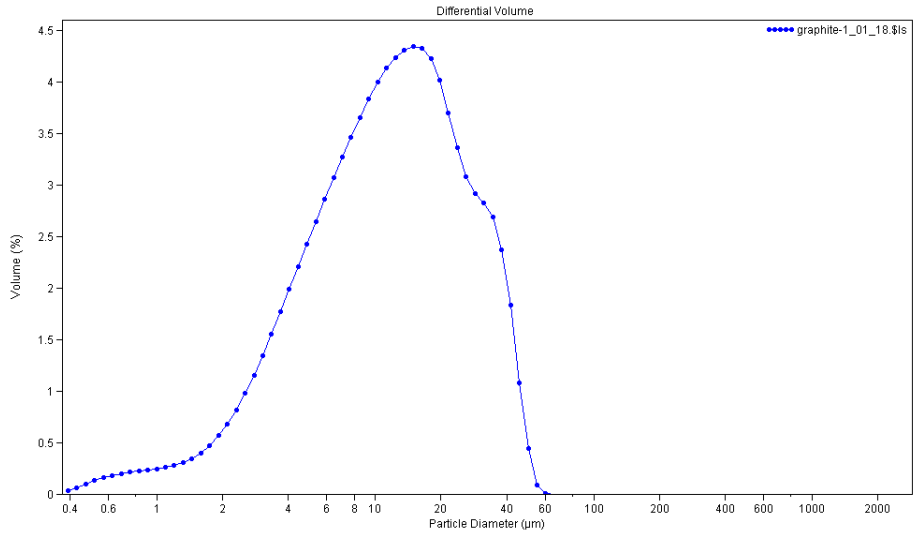

Fig.9. Graphite powder particle size distribution.

Fig.9. Shows the size distribution of the graphite powder, with an average particle size of 14.32 µm. Again there is seen to be a wide particle size distribution within the powder, this may be due to graphite's morphology along with potential agglomeration issues.

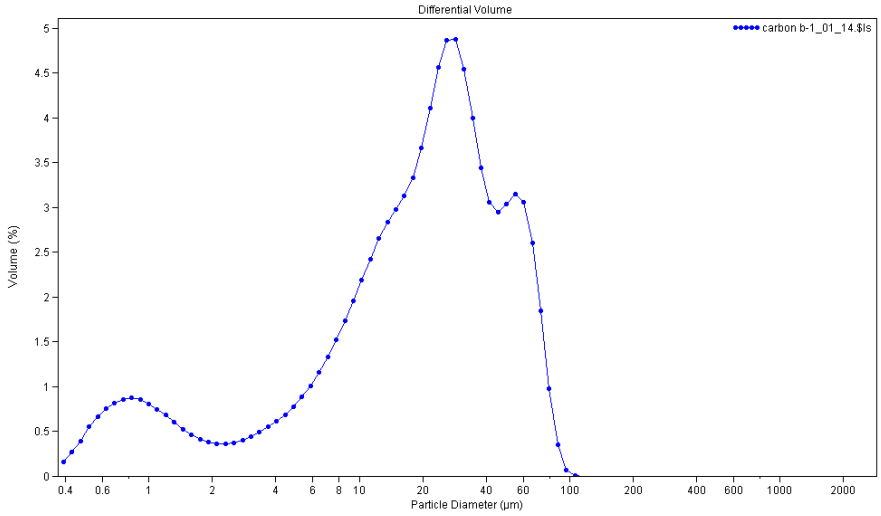

Fig.10. Carbon powder particle size distribution.

Fig.10. Shows the particle size distribution for carbon showing a 22.5 µm average particle size, this was much larger than expected, and along with the shape of the graph suggested agglomeration of particles within the sample.

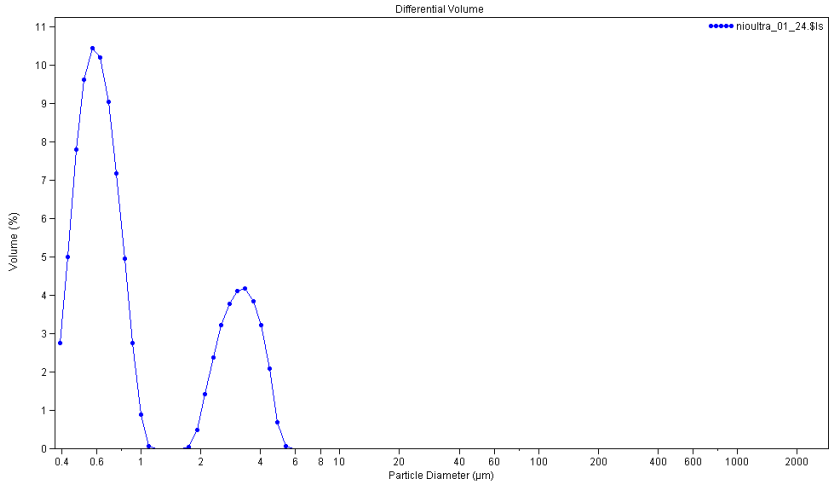

Fig.11. NiO powder particle size distribution.

Fig.11. shows a bimodal size distribution for the NiO powder, the laser diffraction gave an average size of 0.768 µm. It can be seen that there was a peak at around 3 µm which was also seen in the graph of the YSZ powder, this suggests either agglomeration of the particles due to attractive Van der Waals forces or possibly some contamination within the sample bath of the LS230.

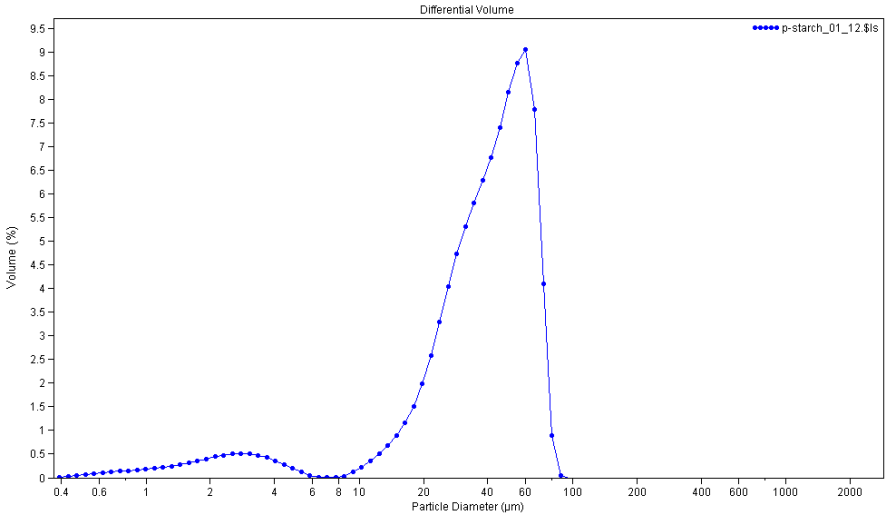

Fig.12. Starch particle size distribution.

Fig.12. shows the distribution for the potato starch powder showing a 40.75 µm average particle size. Again as with the NiO and YSZ powders there is a smaller peak at 3 µm suggesting that there was possibly some contamination in the LS230 bath during analysis.

3.1.4. SEM

Scanning electron microscopy (SEM) is a form of high magnification microscopy used to accurately examine samples down the nanometre scale. It operates unlike optical microscopes by firing a beam of electrons at a sample rather than a beam of light. The beam when contacting the sample then emits x-rays, back scattered electrons and secondary electrons, these are then detected by various detectors and converted into an image which is collected and displayed digitally.

3.1.5. Method

Due to the difficulties experienced with dispersing the YSZ powder and the apparent peaks at around 3μm seen in several of the size distributions SEM was carried out on powders to verify the results of the laser diffraction tests. Analysis was carried out using a Philips XL30 ESEM operating at 15kV, all images taken were secondary electron images.

Samples were mounted on SEM stubs by using sticky carbon dots, a small amount of the sample powder was placed on the carbon dot, excess powder was then blown off using compressed air. To aid conductivity and allow the electrons to flow freely towards the ground, the samples were all sputter coated using platinum. Secondary imaging was used as only one material was present in each sample and as the samples were still in powder form this would yield the clearest images.

3.1.6. Results

Fig.13. and Fig.14. show the SEM images of the YSZ powder, from Fig.13. it appears that the YSZ particles are very large in size with spheres around 10-50 μm being visible. On the left of the image can be seen one of these large spheres which has fractured, this structure is typical of spray drying.

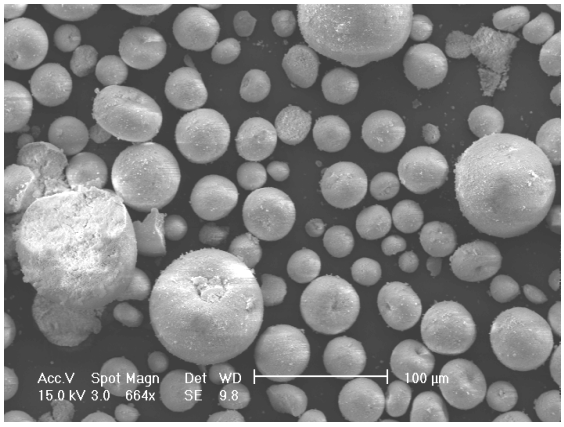

Fig.13. SEM image of agglomerated YSZ particles

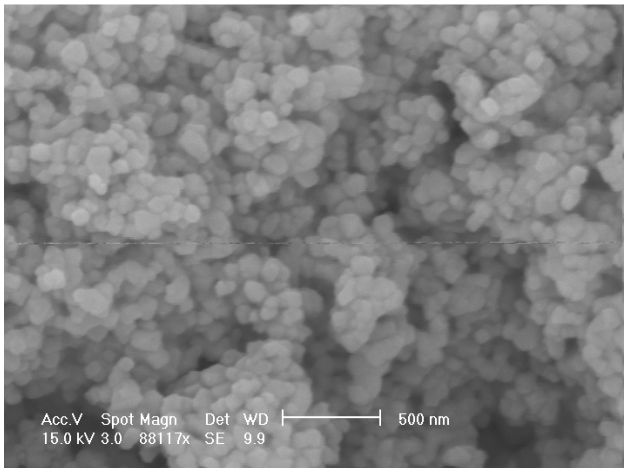

Fig.14. SEM image of YSZ particles

The fractured section was examined at greater magnification as shown in Fig.14., it can be seen that the primary particles are actually around the 0.6 μm diameter as specified by the manufacturer. The larger particles seen in Fig.13. are due to the agglomeration of YSZ particles during the spray drying process, the difference from the specified particle size given by the manufacturer is probably due to the size of the feedstock being quoted rather than that of the resultant spray dried agglomerated particles.

SEM analysis was carried out on all remaining powders and verified the particle size established during laser diffraction. Fig.15. shows an individual carbon particle, whereas Fig.16. shows a collection of flour particles, there can be seen to be two distinct types of particle within the flour sample, those which are spherical and those which are not. Upon closer examination it was seen that the non spherical particles are actually spherical particles with small pieces of debris on the surface. Both agree with the average size found using laser diffraction. Further pictures of the other powders used in this study can be seen in Fig.A and Fig.B. in the Appendix. The average sizes found using both methods can be seen in Table 1.

Material	SEM Size µm	Laser diff size µm
NiO	~1	0.768
YSZ	~0.6	0.627
Carbon	~15	22.5
Flour	~70	63.2
Graphite	~10	14.32

Table 1. Average particle size of powders

It should be noted however that the average particle sizes found using laser diffraction were based up the volume percentage of particles within the distribution, whereas the SEM sizes were based on the numerical number of particles of a specific size. The differing methods and agreement of results leads to a more accurate estimation of the average particle size found within the powders.

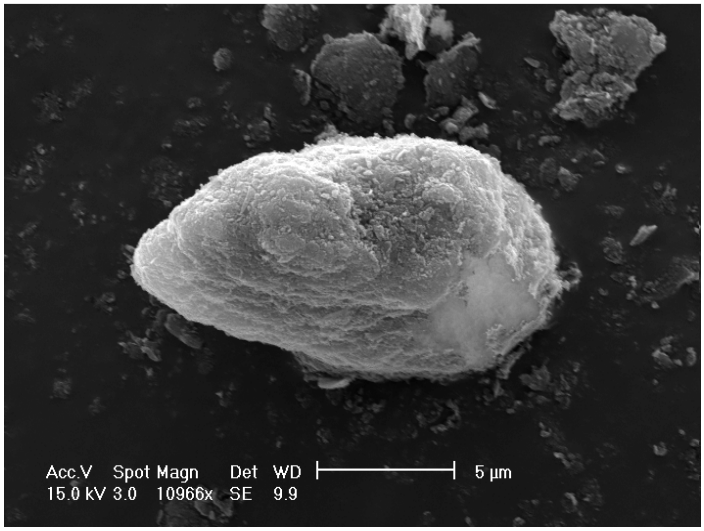

Fig.15. SEM image of an individual carbon particle

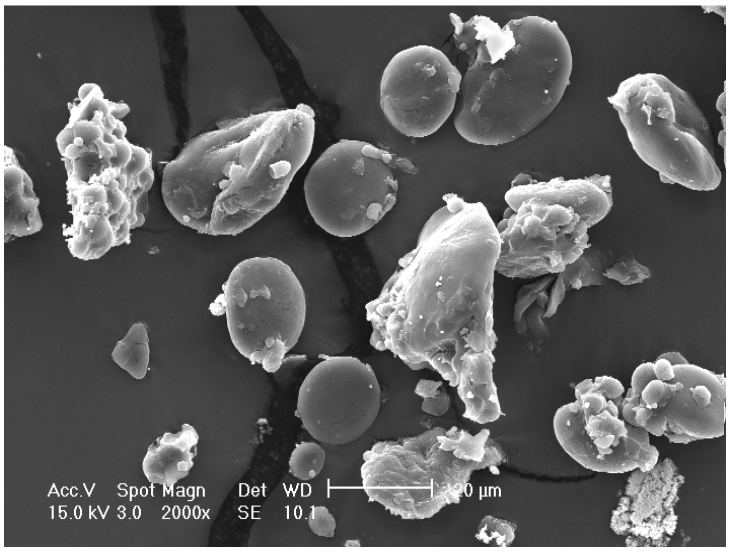

Fig.16. SEM image of a collection of flour particles.

3.1.7. Binder materials

The different components of the binder system used within this investigation were not modified before use. A non-aqueous binder system was used with the following components:

Cyclohexanone – solvent and main organic binder, slightly less volatile than water and less sensitive to changes in environmental conditions. (VWR international LLC)

Polyvinyl Butyral (PVB) – minor binder used to minimise phase separation by increasing the liquid viscosity of the binder system. (Acros organics)

Stearic Acid – a carboxylic acid which acts as a lubricant and dispersant by forming a layer over the constituent powder particles, inhibiting agglomerations and decreasing friction between particles. (BDH chemicals Ltd.)

Dibutyl Phthalate – used to increase the plasticity of the material and reduce brittleness when dry. (Aldrich)

3.2. Initial experiments

3.2.1. Play-doh

The rheologies of the pastes used within this investigation were well matched, this was due to the operation of the twin roll mill only allowing a very narrow band of solid loadings where pastes will be formed, less and the paste is too liquid, any more and the powders fail to form a paste. However to become familiar with the Instron 4467 load frame which would be used to press and extrude the SOFC pastes before sintering, initial runs were carried out using play-doh. Play dough is a dough mixture containing mainly flour and water with a small amount of salt and oil added, plus a colouring agent. As well as familiarisation with the equipment this also allowed paste characterisation to be carried out by application of the Benbow Bridgwater equations.

3.2.2. Method

Material was extruded using a ram, barrel and die assembly where the ram of the barrel was driven by an Inston 4467 load frame coupled with a 30 kN load cell, this arrangement allowed the displacement and load to be measured simultaneously. A schematic of this process can be seen in Fig.17.[38]

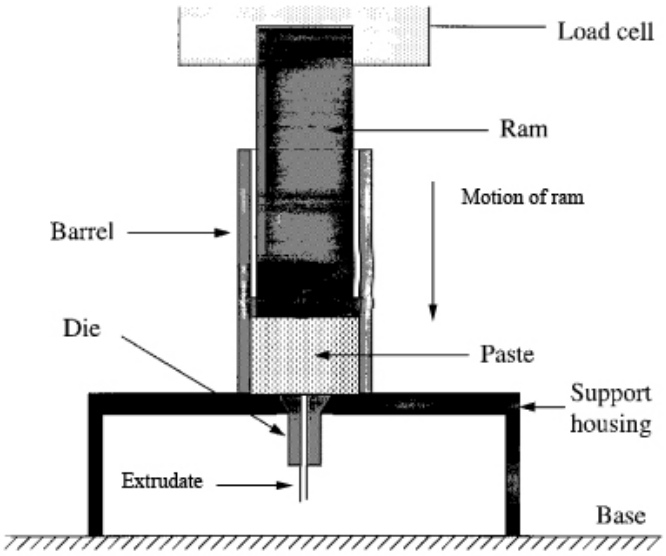

Fig.17. Extrusion schematic[38]

In order to extrude the play-doh it was rolled into small balls which were placed into the barrel and then tamped down using a wooden stick to remove any excess air within the barrel. When filled the ram was placed in the barrel and the assembly loaded into the Instron 4467 load frame and a pre-programmed test was run. This moved the ram at varying speeds starting at 50 mm/min until paste flowed from the die then slowing to 1mm/min before ramping up in steps of 1, 2, 5, 10, 20 & 50 mm/min. The ram ran for 10mm at each of the speeds. The purpose of moving the ram at high speed to begin with is to rid the system of any air pockets which may have been present and fully compact the system.

Initially the test was carried out with a die of 3 mm diameter and 3 mm length. With the test completed the play-doh was emptied from the barrel, the die changed, and the barrel loaded again and loaded into the Instron, this was carried out for dies with length/diameter ratios of 8 & 16 all with 3mm diameter. From this data the rheological properties of the paste were characterised by applying the Benbow Bridgwater equations.

Indent testing of the material was also carried out, this is a simple test where a cone, the apex of which is just in contact with the surface, is released from a test rig and rests on the surface of the material for a set period of time, during this time the cone penetrates into the material. A schematic of the set up can be seen in Fig.18.[32]

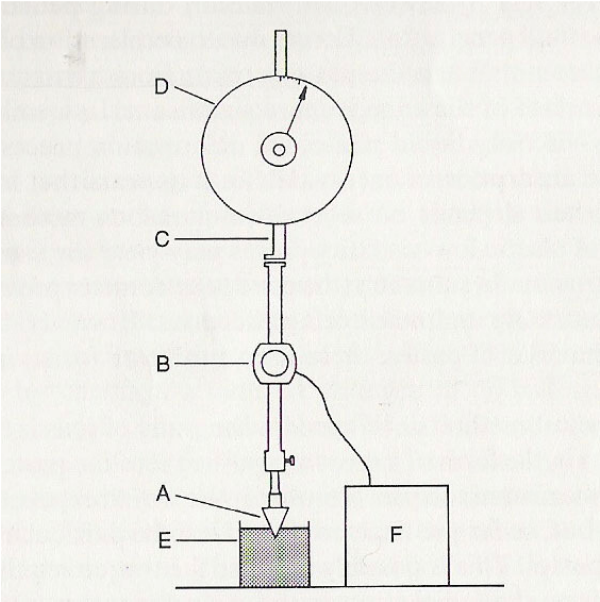

Fig.18. Cone penetration schematic[32]

The equipment seen in Fig.18. being [A, cone; B, low friction bearing; C, rack operated following mechanism; D, scale; E, paste container; F, unit locking cone after set time[32].]

The depth of penetration, the weight of the cone assembly along with the impact angle of the cone can be put into the following equation to find the yield stress of the material:

$$\sigma_c = \frac{F}{(\pi E^2 \tan^2 \mu)}$$

Where:

σ_c = cone penetration yield stress MPa

F = weight of the cone assembly kg

E = depth of penetration m

μ = cone angle rad

This yield stress can then be compared to that found using the Benbow Bridgwater characterisation and has been shown within ideal materials to correspond to the bulk yield stress of the material[32].

3.2.3. Indent testing results

Indent testing of the play-doh was carried out using a Setamatic Penetrometer MKVI using three different cones of varying impact angle and mass, they were left to indent the surface for 15 seconds, the results can be seen in Fig.19.

As can be seen from Fig.19. as the cone angle becomes greater the yield stress decreases, this is due to the material being used not being ideal, in that it was not homogeneous and required mixing due to it drying out in storage.

One problem with this equation is that it does not take into account the amount of time the cone is in contact with the surface of the material, this has a significant impact on the yield stress, as the longer the cone is allowed to be in contact with the surface the deeper the penetration of the cone. For stiffer materials with a high yield stress the time factor is not that great an issue as the cone has very little penetration into the material, however for softer materials with a low yield stress such as play-doh time becomes an important factor.

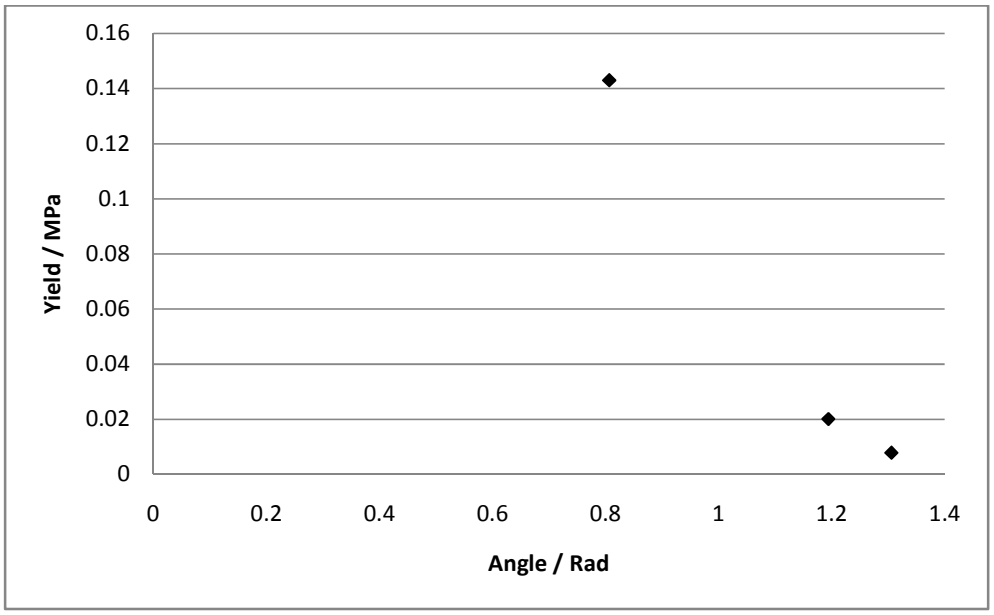

Fig.19. Yield stress vs. Cone angle for varying cones.

3.2.4. Extrusion results

Extrusions of the play-doh led to graphs of the load versus the compressive extension for each die, these can be seen in the Appendix Fig's C, D and E. The data from these graphs was then converted into pressure within the system, these pressure values were then plotted against the L/D of the dies and the best fit lines extrapolated back to zero to give estimated values for pressure at a theoretical L/D of zero, shown in Fig.20.

The values for pressure were then plotted against the die exit velocity for each die used along with the values for L/D zero found in Fig.20. and presented in Fig.21. The values taken from this graph were used to give an estimated value for the pressures seen at v = $0ms^{-1}$ which can be seen presented in Fig.20.

The Benbow Bridgwater equation Eqn.1 shown in section 2.4. of this report was then re-arranged to the following four equations. The values for A,B,C and D were taken from the points labelled in Fig.20. The resultant values gained from these equations can be seen in Table2.

σ_o - Bulk yield stress MPa Eqn.3.

$$\sigma_0 = \frac{A}{2\ln\left(\frac{D_o}{D}\right)}$$

α - Die entry velocity factor Pasm^{-1} Eqn.4.

$$\alpha = \frac{B - A}{2\ \ln\left(\frac{D_0}{D}\right) \times Vmax}$$

τ_o - Die wall initial yield stress MPa Eqn.5.

$$\tau_0 = \frac{C - A}{4\ \frac{L}{D}}$$

β - Die wall shear stress velocity factor Pasm^{-1} Eqn.6.

$$\beta = \frac{(D - B) - (C - A)}{4\left(\frac{L}{D}\right) Vmax}$$

Parameter	σo	α	To	β
Value	0.06	2.14	0.02	0.68

Table 2. Play-doh Benbow Bridgwater paste parameters.

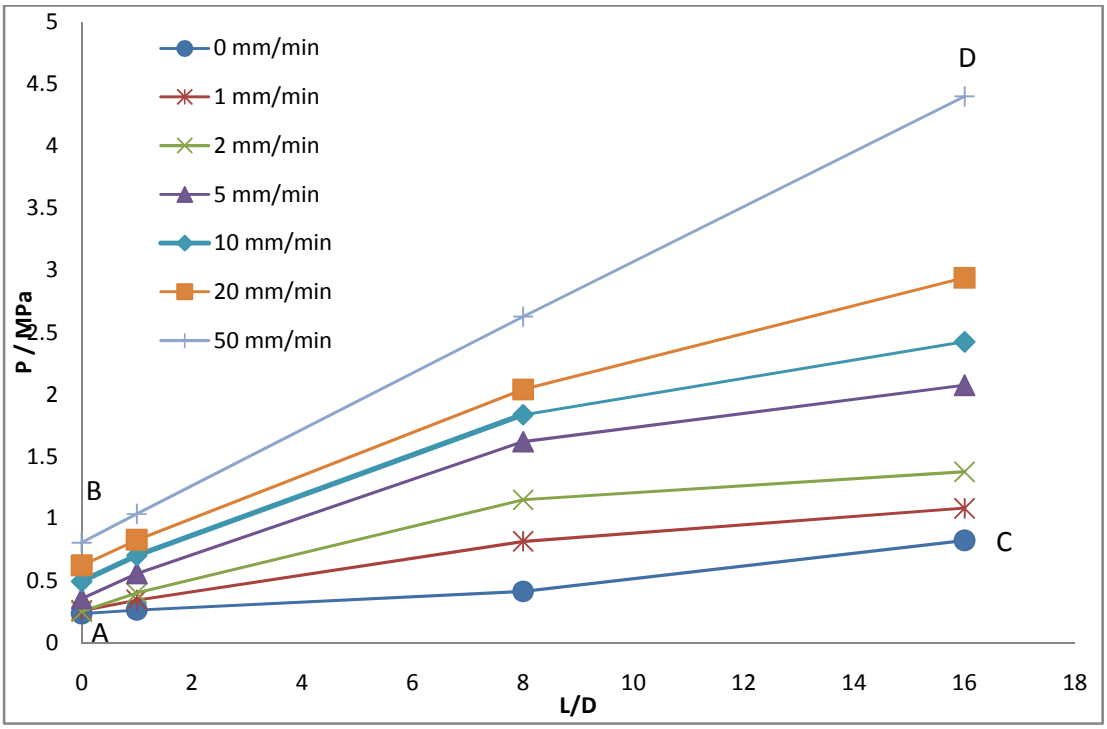

Fig.20. Plot of Pressure vs. L/D for all velocities.

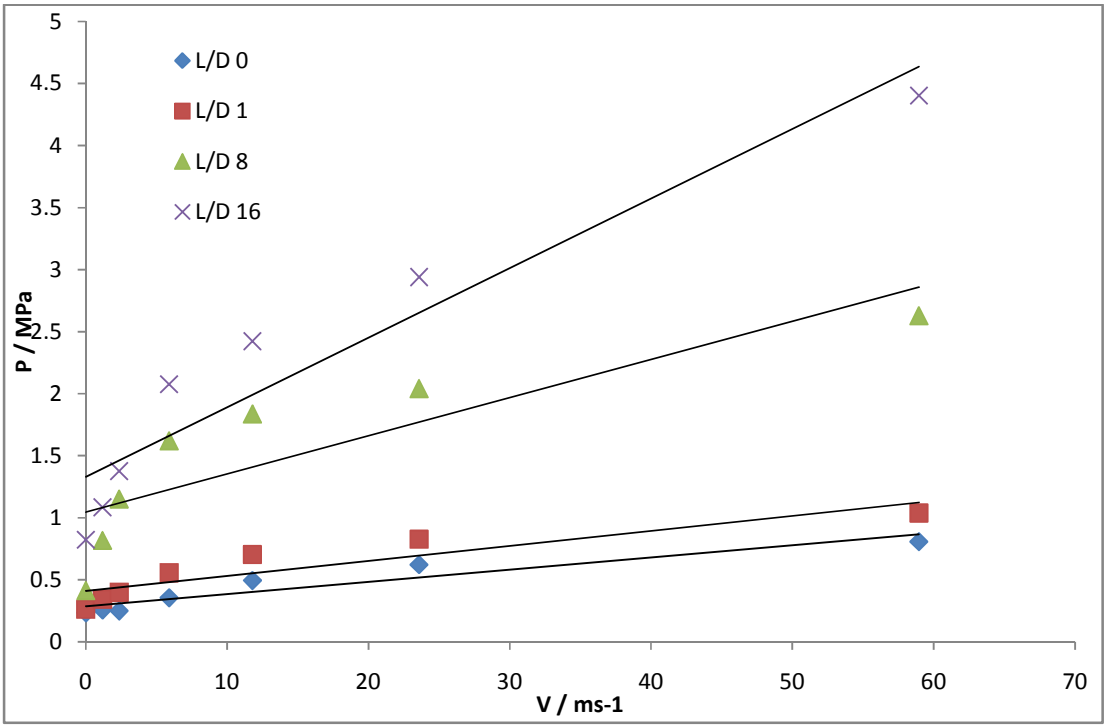

Fig.21. Plot of Pressure vs. V for all L/D showing the 4 parameter fit

The bulk yield stress according to the Benbow Bridgwater characterisation was 0.06 MPa comparing this to the values achieved using the indent test rig which can be seen in Fig.19. 0.06MPa can be seen to lie around mid way on the graph suggesting that this is a reasonable estimate for the yield stress of the material.

The curvature of the graph in Fig.21. suggests that a 6 parameter characterisation is more suitable for this material. For the purpose of comparison to the yield stress gained from indent testing the 4 parameter characterisation was suitable however it will have overestimated the yield stress slightly.

3.3. Porosity forming agent (PFA)

From the literature review several suitable porosity agents were identified these can be seen in the raw materials section, this is the sacrificial material that will pyrolise during the sintering process leaving the body with a porous structure. Carbon black, which was previously used by Powell[22] was the first agent identified along with graphite, potato starch and wheat flour. These materials have been identified and used in several studies previously with varying levels of success so were known to be clean burning which was a requirement along with having a low cost which is an important consideration in the manufacture of SOFC anodes.

3.3.1. PFA testing

In order to evaluate the suitability of the indentified PFA's several small pressed pellets of the materials were prepared using the same formula as the final SOFC tubes and sintered. This reduces processing time taken to prepare and evaluate pastes as well as requiring less raw materials and reducing costs. The sample was first prepared as a slurry of the

constituent powders to aid better mixing than if they were dry mixed, they were prepared using the formula given in Table 3.

Ingredient	**Mass (g)**
YSZ	4.2
NiO	16.8
PFA	9
Binder (Water)	Approx 20

Table 3. Pellet formulation

The slurry was then dried in an oven at 80°C for 2 hours, removed and placed into a pestle and mortar where they were ground. These ground powders were passed through a 400 μm sieve, any coarse fractions were reground in the pestle and mortar until they passed through the sieve. The resulting powders were then pressed into pellets using an Instron 4467 static load frame with a 30kN load cell and a pellet die press with an 8.5 mm diameter.

The Instron was run at 0.5 mm/min, initially to a force of 0.2 kN and stepping up in 0.2 kN steps to 2 kN. This was to determine at which load pellets are formed and stable enough to sinter. The compression in mm was recorded for each load and then plotted, where the gradient of the graph began to decrease suggested the best force at which to produce pellets as after this force compression of particles was no longer taking place. For each PFA sample 1g of dry powder from the samples prepared using the formulation in Table 2. were used to press individual pellets.

After pressing the resultant pellets were sintered in a Carbolite furnace using a programme similar to that which was used to sinter the final SOFC tubes:

Debinding Room Temperature-600°C 7 hours

Dwell 600°C 2 hours

Sintering 600-1350°C 8 hours

Dwell 1350°C 2 hours

Cooling 1350°C –Room Temperature 22 hours

3.3.2. Results

Fig.22. shows how much compression took place when various forces were applied to the powders containing carbon PFA within the press. The graph shows that, at 2 kN of force the compression is at around its maximum suggesting this would be an adequate force to apply to form pellets.

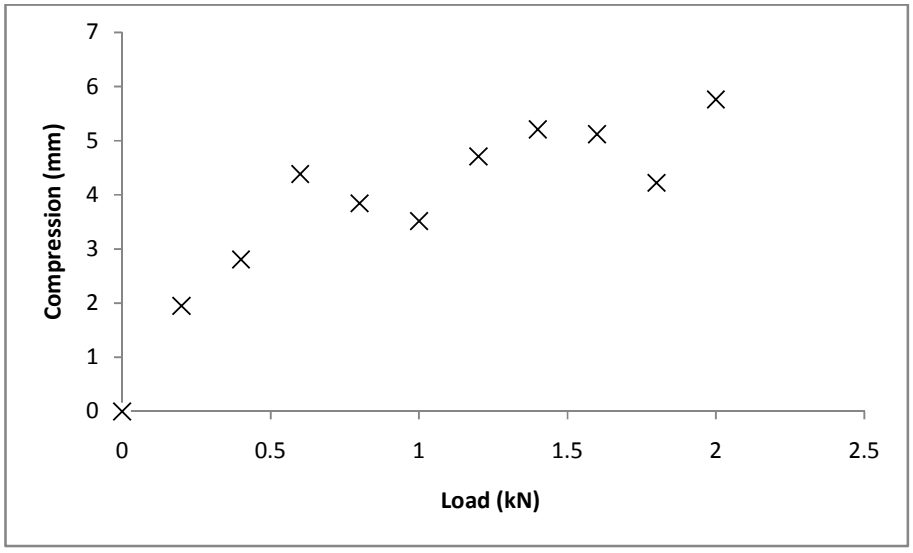

Fig.22. Compression vs. Load observed during pellet pressing

During pressing of the pellets it was seen that the powders containing carbon, flour and graphite as PFAs all compressed sufficiently to form pellets that are stable enough to be sintered at 2 kN of force. Pellets containing potato starch as a PFA did not forms pellets at 2 kN to remedy this the compressive force was increased progressively up to 10 kN, at this

force suitable pellets were still not formed. It was observed that when pellets were removed from the press a “pinging” noise could be heard, this suggested that the particles were elastically deformed during the pressing and were returning to their former shape and size when the force was released. To overcome this approximately 0.1g of glycerol was added to 1g of dry powder to form the pellets containing potato starch.

In Fig.23. the un-sintered pellets can be seen. As well as the previous problems due to elastic spring back seen in the PFA starch pellet previously, end-capping in the PFA graphite pellet was also noticed, which is again caused by elastic deformation of particles within the pellet.

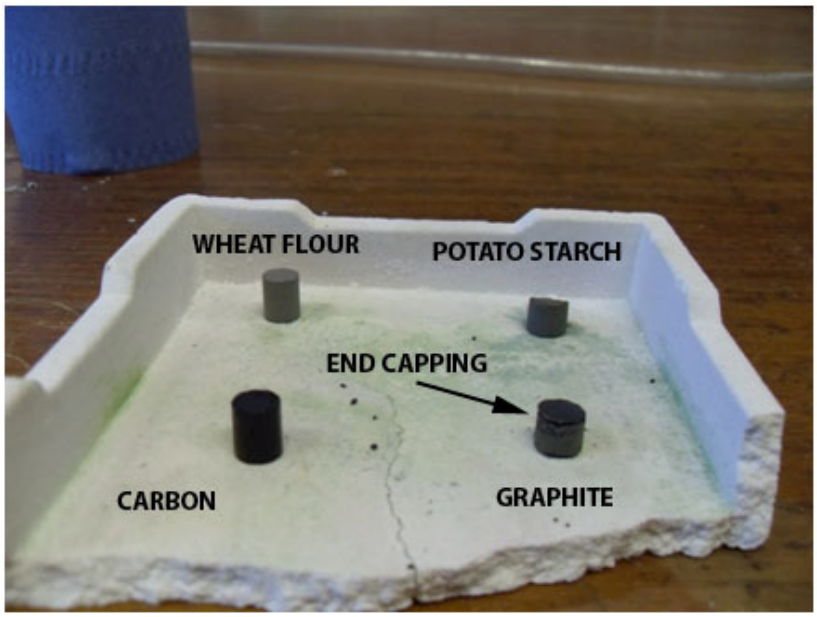

Fig.23. Un-sintered pellets containing different PFAs

Upon completion of the sintering programme the pellets were removed as can be seen in Fig.24. The first thing observed was that the pellets have turned green upon sintering, also that there has been vaporisation and deposition of the NiO powder which can be seen by the blue areas surrounding the pellets this was probably due to the different oxidation states of the NiO after sintering.

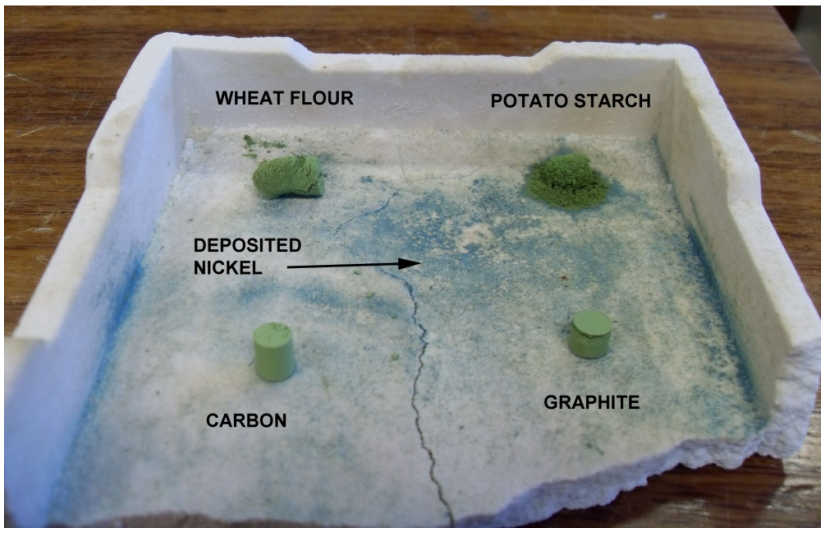

Fig.24. Corresponding sintered pellets.

From Fig.24. it can be seen that the graphite and the carbon both retained the pellet shape well, but also with very limited visible pores over the surface. The wheat flour produced a less hardy but with very good porosity visible over the surface, suggesting that it may be a suitable material for use with SOFC's. The potato starch was seen to not form a cohesive pellet, this poor performance combined with the difficulties in processing the potato starch and forming the initial pellets meant it was discarded as a possible PFA.

Due to the fact it is natural material a small sample of wheat flour was pyrolised in the furnace at 1350°C to observe the amount of residual ash remaining. There was seen to be less than 0.01% of the material left as residue suggesting that it could be suitable as a PFA as it does not leave large amounts of material after sintering which could interfere with the SOFC operation.

3.4. Powder processing

3.4.1. Milling

High energy ball milling has been shown to improve the uniformity of processed powders, and so was applied to a mix of the three constituent powders for a 24 hour period. Due to the operation of the ball mill and health and safety issues the mill could only be run for 8 hours a day, the 24 hour processing time therefore taking 3 days to complete.

It was noticed that after the 24 hour processing period that there were issues with moisture in the system meaning that the powders agglomerated into a large mass at one end of the ball mill. This meant that material inside this agglomerated mass had little interaction with the milling media and thus no particle size refinement or mechanical alloying had taken place. This was verified using laser diffraction which showed that there had been little if any effect on particle size this suggested that the agglomeration had happened early on in the milling process.

To overcome the problem of excess moisture within the mill, drying of the powders beforehand would need to be carried out. However ball milling already suffers from long processing times, this increase in time to dry out powders would make the process unviable for the investigation. An alternative to ball milling was a high power TEMA mill which would be capable of processing smaller batches of powders, in much shorter time frames. All subsequent trials took place using a TEMA mill.

3.4.2. Method

The TEMA mill works by exciting a pot containing several rings of different sizes with a central solid disc. Before use the mill needs to be cleaned using sand to avoid contamination of samples. The sample material sits between these rings which mill the powder as the pot is excited and oscillated by a sprung eccentric motor.

Fig.25. TEMA mill showing internal rings[39]

Within this investigation a small sized pot with two rings and one central disc was used, this had the capacity to mill up to approx. 100g of material per run. The pot used, minus lid showing the internal rings and disc with space between for samples can be seen in Fig.25.[39]

The main advantage of TEMA milling over ball milling is the short processing times, a sample of powder containing carbon PFA made using the formulation in Table 4 was placed in the mill, the mill was stopped and samples taken at 1,2 and 3 minutes respectively. After milling the samples were taken and analysed using laser diffraction to establish the particle size and particle size distribution. With powders initially ranging in

average size from 0.4 μm up to 64 μm the aim of milling was to significantly reduce the range of sizes to achieve 100% of particles under 10 μm in size.

Ingredient	Mass (g)
NiO	30.5
YSZ	6.9
Carbon PFA	20vol%

Table 4. Milling formulation for carbon PFA sample

3.4.3. Results

After milling samples were analysed using laser diffraction as described previously, the effect of milling on the powders could be seen visually with the powders in suspension of 100:1 water and Dispex solution prior to laser diffraction. The non milled powder was seen to separate into layers with the lighter carbon floating on the surface after a short period of time around 30 seconds. The milled powder however remained well mixed and held in suspension for over 15 minutes.

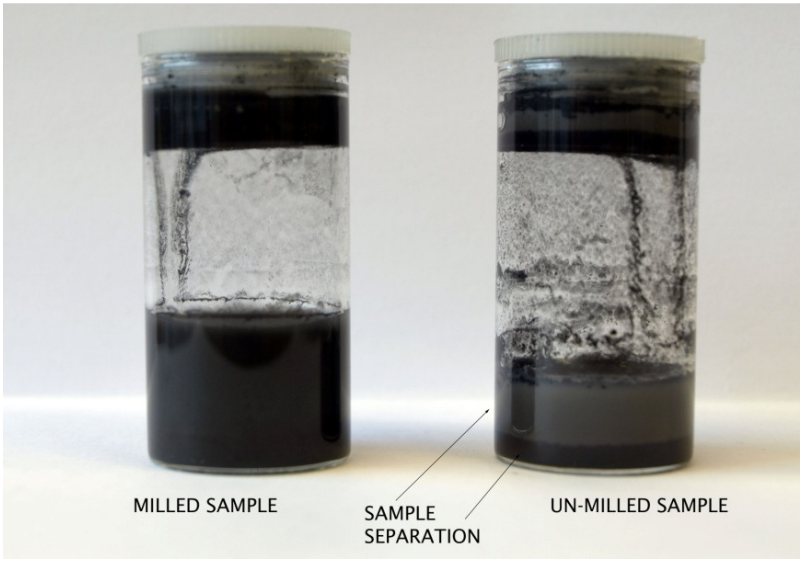

Fig.26. NiO YSZ and carbon Powders in suspension.

Fig.26. shows the powders in suspension after 15 minutes. The tube on the right contains the un-milled sample and on the left the milled sample. It can be seen that the un-milled sample has completely sedimented whereas the milled sample is still well mixed and suspended.

Laser diffraction size analysis showed that the un-milled mixed powders had a mean average particle size of 12.8 μm with only 54.1% of particles being under 10 μm in size as seen in Fig.27. After 3 minutes of TEMA milling the average particle size had been reduced to 3.38 μm with 100% of particles being under 10 μm in size as seen in Fig.28., meaning a finer particle size distribution with the peaks of the bimodal graph moved closer together.

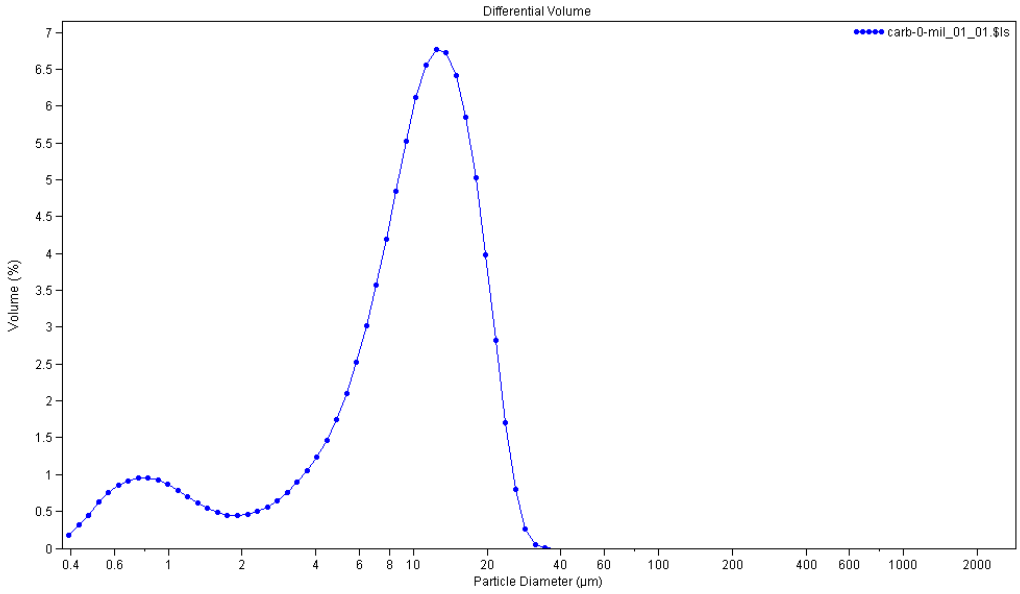

Fig.27. Un-milled carbon NiO YSZ mixed powder size distribution

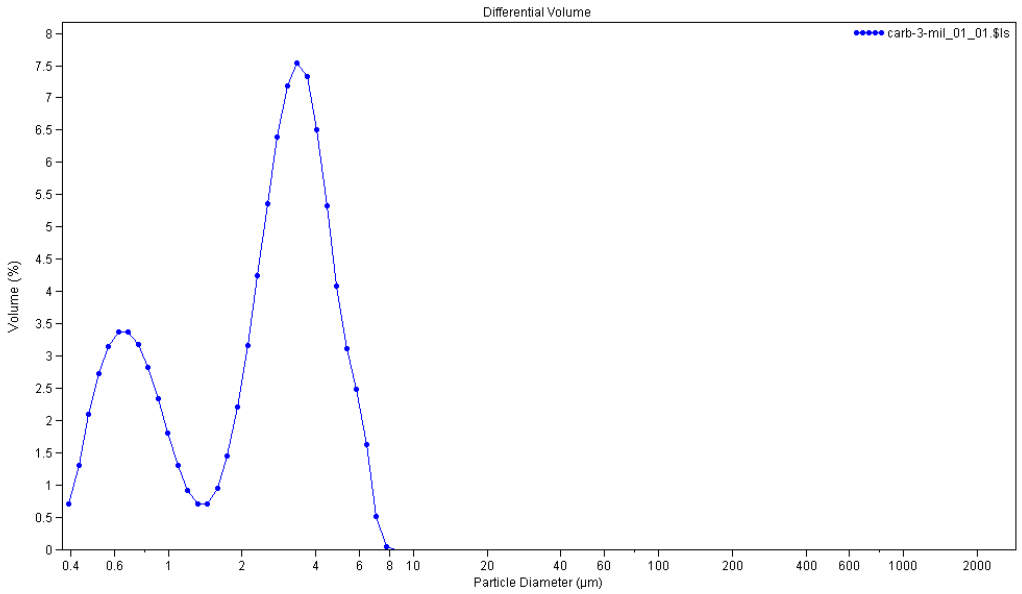

Fig.28. Milled carbon NiO YSZ mixed powder particle distribution.

With the powders visually being more uniform and dispersing better along with the laser diffraction showing that 100% of particles being under 10 µm in size it was decided to process all powder mixes for 3 minutes. This was also advantageous as due to the high energy of the TEMA mill it heats up greatly during milling due to the movement inside and friction. If the powders were processed for much longer there may have been issues with the powders becoming too hot and affecting the constituent particles such as flour.

With the milling time established at 3 minutes, three batches of powders were prepared using the formula in Table 5 and then milled for 3 minutes ready for preparation as pastes. One batch of powder was prepared for each PFA, those being wheat flour, carbon and graphite.

Ingredient	**Mass (g)**
NiO	122.1
YSZ	27.9
PFA	20vol%

Table 5. Milling formulation for all powders

3.5. Paste preparation

Pastes were prepared using a bridge twin roll mill, which uses high shear forces to mix stiff pastes with high solid loadings. It operates by two counter rotating rollers moving at two different speeds, material is loaded into the top of the mill and is then forced between the two rollers, as more material is added the gap between rollers can be expanded to allow for larger batches to be processed. As the solid and liquid phase mix the liquid phase tends to move towards the edge of the rollers which must be removed using a spatula and then placed back onto the rollers to aid better mixing.

When sufficiently mixed due to the differing speeds of the rollers the paste should move onto the slower moving roller, at this point the paste is cut, removed, folded and then added back into the top of the mill. This is done again to better aid mixing, and should be repeated until the paste is a suitable consistency. When ready the paste is cut and then removed from the roller and stored in ready for use.

3.5.1. Paste preparation

3.5.2. Method

Seven different pastes were made in small batches sufficient to fill the barrel of the extrusion device once, this was done to reduce waste of materials and as working with smaller batches on the twin roll mill is more user-friendly. Prior to loading onto the mill powders were first mixed by hand using a metal stirrer within a fume cupboard until uniform in colour, the liquid stage of the binder was then added in small amounts and mixed in until absorbed and as much dry material formed into a solid mass as possible.

Seven different pastes were made, one containing pure YSZ which was used as the central layer within all tube extrusions. Three pastes were made containing mixtures of the

constituent powders with the three different PFAs in their un-milled state, and three pastes containing mixtures of the constituent powders with the three different PFAs in their milled state.

All pastes were made using the same ratio of NiO, YSZ and PFA that is 80%wt NiO to 20%wt YSZ and then 80% vol NiO YSZ mix to 20%vol PFA. The exception to this was the pure YSZ paste which was made up of 100% YSZ powder. The formulation used for each batch of paste can be seen in Table 6, and the binder formulation which remained constant for all pastes can be seen in Table 7.

Ingredient	Mass (g)
NiO	30.5
YSZ	6.9
PFA	20vol%

Table 6. Powder formulation for all pastes

Ingredient	Mass (g)
Cyclohexanone	6.375
Di-butyl phthalate	0.225
PVB	5.625
Stearic Acid	0.1125

Table 7. Binder formulation for all pastes

The combination of powder and binder content lead to a soft paste, which began to stiffen due to the cylcohexanone being milled and worked evaporating from the mixture, to remove enough cyclohexanone to form a suitable paste would take a large amount of time. The formation of a soft paste was favourable as adding liquid after mixing had began on the mill was not possible. To stiffen the pastes 10g of dry powder was made using the same ratios as seen in Table 5 and added gradually until the paste was a suitable constituency for use within the extrusion process.

The pastes were mixed for between 10 and 20 minutes depending on the materials used as the pastes containing differing porosity agents behaved differently with some mixing faster than others. During mixing softer material containing more liquid phase has a tendency to move towards the edge of the rollers, to remedy this and improve mixing it was necessary to manually remove the paste using a metal spatula and move it to a more central position on the rollers.

When the pastes had sufficiently mixed and started to form one large homogenous sheet uniformly covering the rollers the sheet was then sliced, removed, folded and passed through the mill again, this was repeated several times to ensure thorough mixing. When ready the paste was sliced using a knife, removed as a sheet from the roller and placed straight into a sealed plastic bag, then into a fridge to prevent the paste drying out before extrusion

During processing it was noticed that the graphite powders were extremely dry and flaked off using the above formulation, this is due to the plate like morphology and large surface area of the graphite causing it to not mix and shear as well as the other PFAs. To remedy this firstly the amount of dry powder being added was reduced by 10% which still lead to a paste not being formed. Secondly the dry powder content was reduced by 10% and the amount of binder being used was increased by 10% to increase the liquid content within the system. The reduction in dry powder, combined with the increase in liquid content lead to a soft paste as with the other powders to which more powder was added gradually until the paste was suitable.

3.5.3. Results

During mixing it was seen firstly that milled powders formed a homogenous suitable paste much faster than the un-milled mixes of constituent powders. This would be expected as during the milling refinement of the particle size mixing would have already taken place, thus reducing the work that the mill has to exert to form pastes. The milled powders also formed pastes with much less user input involved in moving soft paste from the edges of the roller to the centre to aid mixing than the other powders. On a purely subjective level the pastes formed using the milled powders also felt better and easier to handle than those made using the un-milled constituent mixed powders.

Secondly it was observed that the powders containing graphite were very difficult to work with and took much longer processing time and effort to form into usable pastes. This is due to the stiffness of the material, and due to the extra time required suggests that the graphite may not be a suitable alternative as a porosity agent as any gains in efficiency will be offset by the extra energy and cost of processing the material at earlier stages of production.

3.6. Tube extrusion

3.6.1. Method

Samples were extruded using an Instron 4467 load frame with a 30 kN load cell as used and described in the play-doh testing section of this report. The barrel and load cell were the same as previously, however the ram had a steel mandrel attached around which the pastes were wrapped and then loaded into the barrel as one, the ram with pastes loaded around the mandrel of 50mm length can be seen in Fig.29.

The die used had a diameter of 2.5 mm and the mandrel a diameter of 2 mm this allowed for tubes with very thin walls to be made. This combination of die and mandrel diameter gave a wall thickness of 0.25 mm with the YSZ and YSZ, NiO PFA cermet precursor having thicknesses of 0.125 mm each.

Fig.29. Pastes wrapped around mandrel of ram.

Samples needed to be loaded onto the mandrel and extruded quickly, as the cyclohexanone used within the binder system is highly volatile and evaporates off quickly causing the pastes to dry out and become too stiff to extrude. For each of the 6 pastes containing the 3 varying PFAs a small sample of the pure YSZ paste was firstly wrapped around the barrel, the NiO YSZ PFA paste was then wrapped around this until the top of the ram was no longer visible, as seen in Fig.29. These were carried out individually with the barrel, ram and die being fully cleaned between each run to avoid contamination of the samples.

As one piece the ram and material were loaded into the barrel and a small brass collar was slid over the mandrel and into the die, this was used to ensure that the mandrel was completely central within the die and that the extrudate flowed correctly out of the die as seen in Fig.30. The barrel and ram were then loaded into the Instron load frame, and the programme was run, to carry out the extrusions a very simple program which simply moves the load frame at 0.5 mm min^{-1} with a safety stop at 30 kN the limit of the load cell was used. The test runs were stopped manually when sufficient material had extruded through the die.

Extruded material was left to dry out slightly for approximately 2-3 minutes at this point due to the stiffness of the material it was snapped into manageable sized pieces approximately 150-200 mm in length by hand. With the extrudate in manageable sections it was then snapped by hand again into lengths of around 30 mm each ready to be sintered.

3.6.2. Discussions

During the first batch of extrusions the brass collar was not used and the mandrel was simply aligned by eye to being central within the die, this lead to uneven extrudate with large surface. In all cases curvature of extrudate was significant. This extrudate was totally unsuitable for sintering as there were no layers and the two materials were seen to be separate from each other on either side of the extrudate, as can be seen in Fig.32.

Due to the failing of this batch of extrudate the brass collar was designed and made in the workshop to allow for the mandrel to be properly centred within the die. This can be seen in Fig.30. and Fig.31., this collar allows the mandrel to only pass through the die centrally, as material starts to pass through the die it forces the brass collar away which then falls off and is collected. Due to the stiffness of the pastes being extruded they then remain centralised until the extrusion is completed.

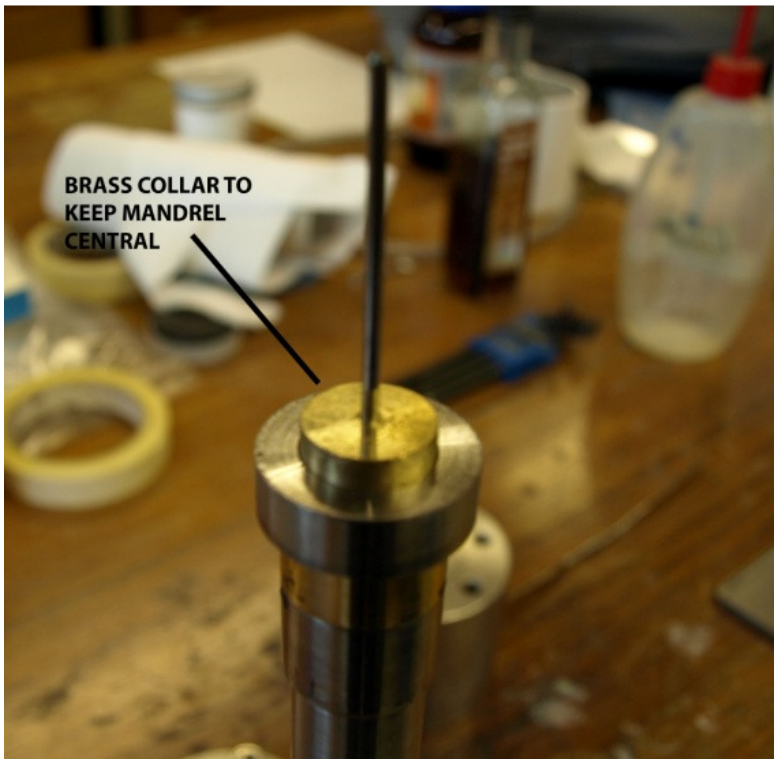

Fig.30. Die with brass collar fitted.

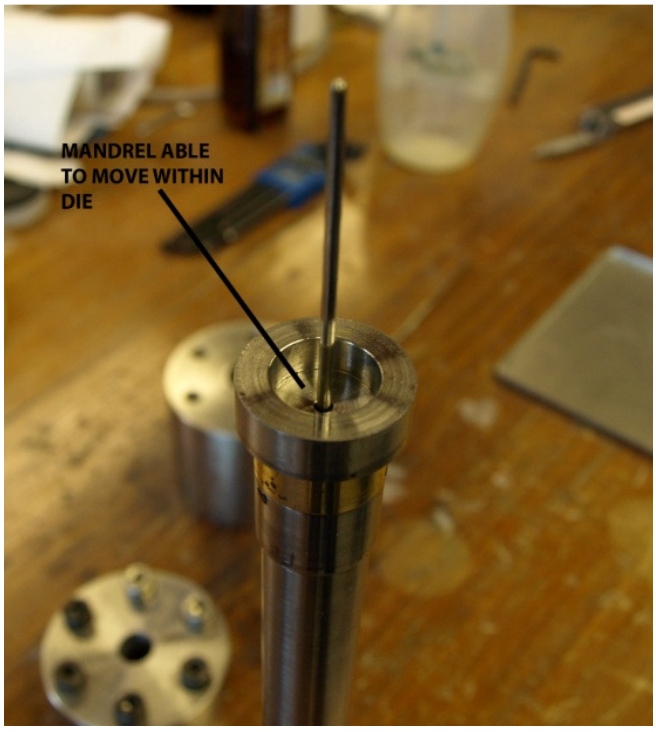

Fig.31. Mandrel through die without brass collar.

With the brass collar in place the pastes were seen to extrude as expected forming tubes with two distinct layers one of YSZ paste internally and the other external layer of the YSZ , NiO PFA cermet. However even using the brass collar surface defects were seen within extruded materials, mainly within the pastes containing graphite.

3.6.3. Results

Fig.32. shows large feathering defects on one side of the tube which have lead to an unusable extrudate, the same was seen within the milled and non milled graphite PFA pastes. This follows on from difficulties in processing the graphite pastes on the twin roll mill and is probably due to the plate like morphology of graphite as a material causing significantly different flow properties.

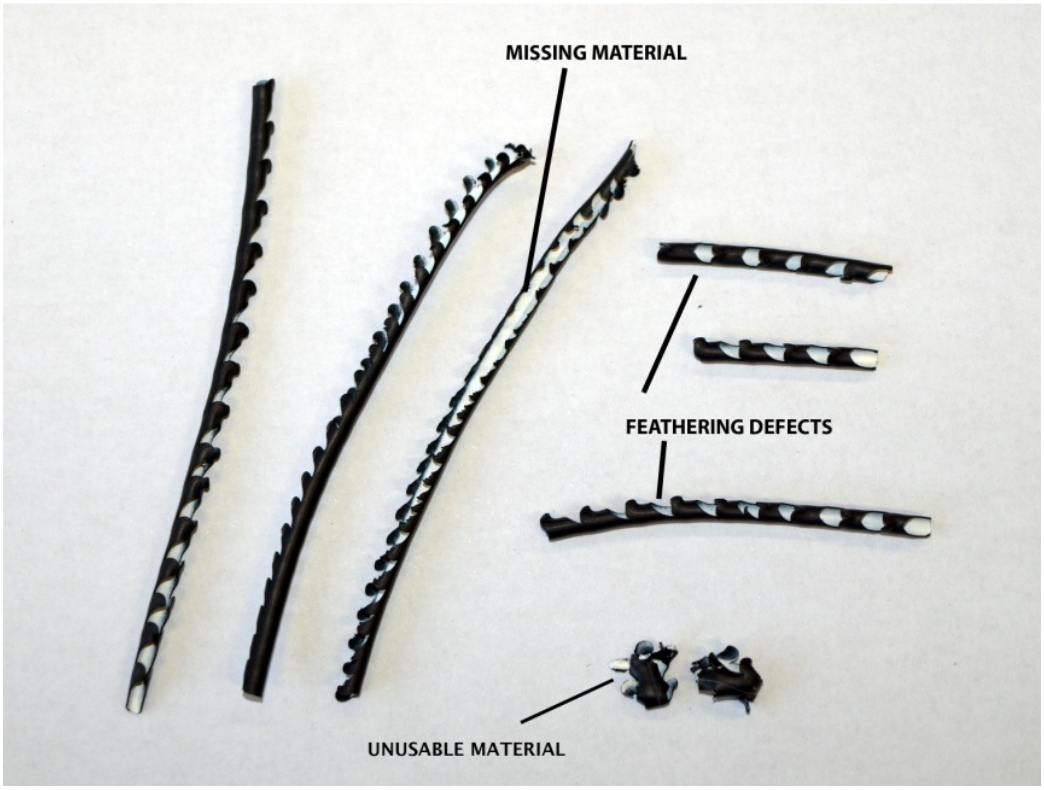

Fig.32. YSZ and graphite PFA paste extrusion defects.

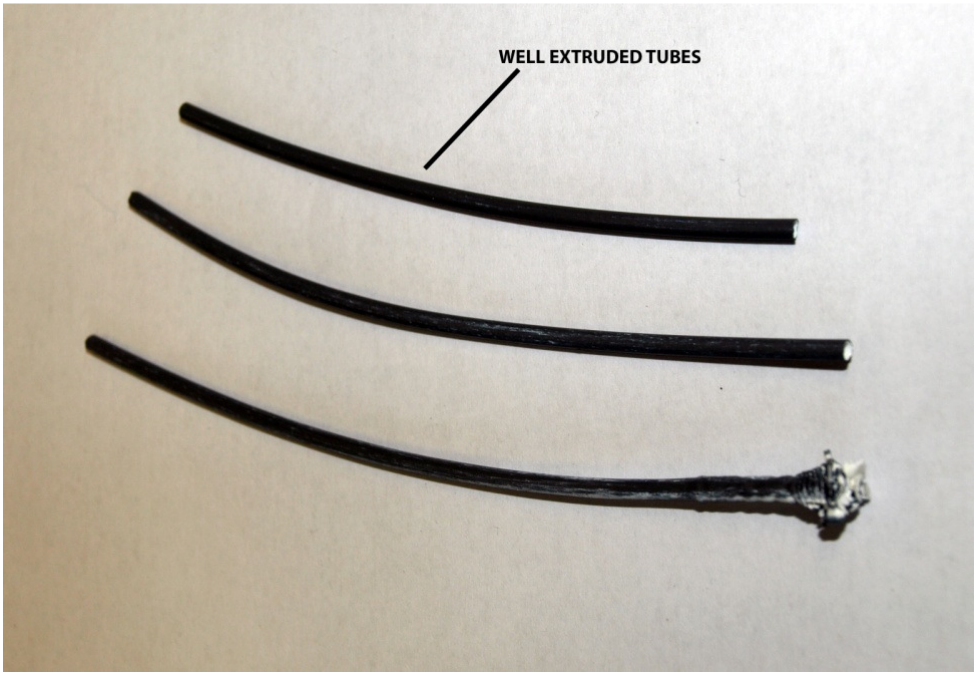

Fig.33. YSZ and flour PFA paste tubes as extruded.

In Fig.32. the varying defects experienced can be seen, with large amounts of feathering, and the absence of one side of the tube. The feathering appears to have been caused by stick slip motion of the ram, it was noticed during later runs that the materials appeared to extrude with fewer defects when run at 1 mm min^{-1} instead of 0.5 mm min^{-1} the Instron appears to be operating with a jerking motion at the lower rate and operating more smoothly at the slightly higher rate.

Fig.33. however shows the properly extruded tubes of around 150 mm in length, the large mass visible is where the paste clumped together whilst pushing the brass collar out of the die and barrel. After this the tubes were seen to extrude as expected, the dark outer layer containing nickel and the white inner layer of YSZ can be better seen in Fig.34. which shows three tubes of approx. 30 mm in length ready to be sintered.

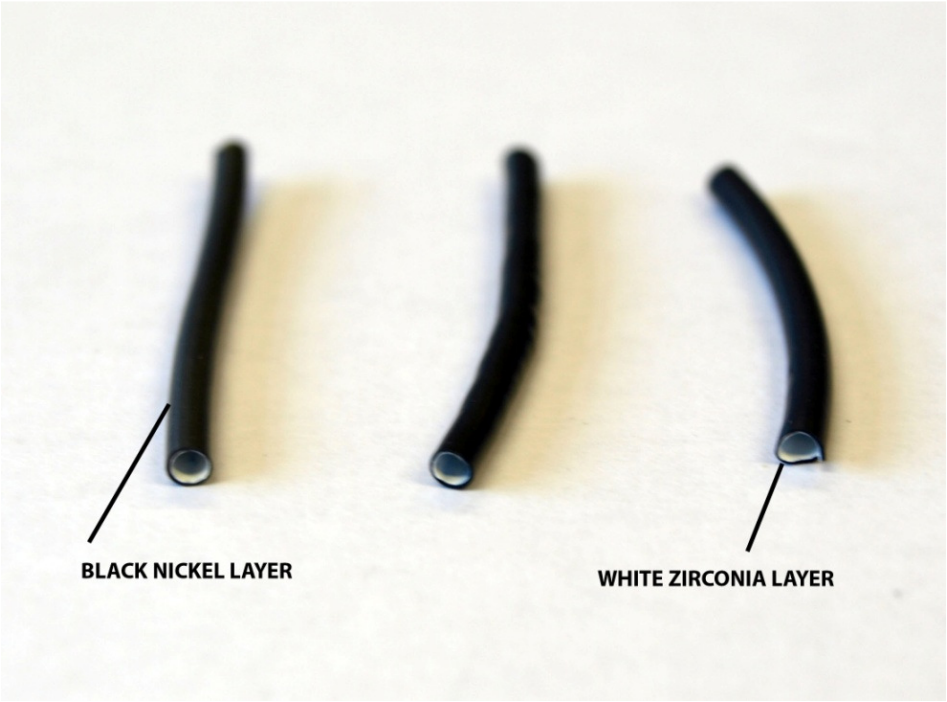

Fig.34. YSZ & carbon PFA tubes ready to be sintered.

During extrusion an average reading was taken for the force required to extrude the various pastes, these can be seen in the table below. From Table 8. it can be seen firstly that the milled paste containing flour was the easiest to extrude requiring the least force, this follows from the flour being the easiest material to form into a paste. It can also be noted that the pastes formed using milled powders required a lower force to extrude than those without milling, the more uniform particle size and distribution again leading to easier processing of the pastes.

Paste	**Extrusion force (kN)**
Flour	13.8
Milled Flour	11.4
Carbon	14.9
Milled Carbon	12.3
Graphite	15.7
Milled Graphite	15.2

Table 8. Extrusion forces for all pastes

Again it can be seen that the paste containing the graphite was the hardest to extrude this is due to the properties of graphite which have been seen to cause difficulties previously, these difficulties suggest that it is an unsuitable material to be used in the manufacture of SOFC anode tubes. However as the materials had already been processed and extruded the graphite tubes were sintered to establish how the graphite acts as a porosity agent.

3.7. Tube sintering

3.7.1. Method

With the pastes extruded they were then cut to appropriate size, around 30 mm in length ready to be sintered. Before sintering all samples, a tube of each non milled material was placed into the Carbolite furnace and sintered using the programme in Table 9.

Process	**Start Temp (°C)**	**End Temp (°C)**	**Time (hrs)**
Drying	Room temp	150	2.5
Dwell	150	150	2
Cooling	150	Room temp	2.5
Debinding	Room temp	600	5
Dwell	600	600	5
Sintering	600	1350	4
Dwell	1350	1350	2
Cooling	1350	Room temp	12

Table 9. Initial sintering programme.

The differing thermal expansion coefficients mean that each paste will expand at a different rate when heated, there are methods to control or overcome these differences. Several layers of material gradually increasing the NiO content and decreasing the YSZ content is the standard method to do this, however due to time constraints within this project this was not possible. The other method would be to increase the time over which the tubes were sintered ensuring that they were heated slowly enough so that the tubes remained in one piece and didn't crack during the sintering process.

When the tubes were removed from the furnace they were seen to still be in one piece however were suffering from slight surface fractures and cracking, however they were still structurally sound. To try and reduce the amount of cracking the sintering programme was altered to that in Table 10.

Process	Start Temp (°C)	End Temp (°C)	Time (hrs)
Drying	Room temp	150	5
Dwell	150	150	2
Cooling	150	Room temp	5
Debinding	Room temp	600	8
Dwell	600	600	5
Sintering	600	1350	8
Dwell	1350	1350	2
Cooling	1350	Room temp	20

Table 10. Modified sintering programme

This was done so that the heating took place over a longer period of time which should reduce the amount of cracking due to differences in thermal expansion. As the materials will still expand and contract however over a longer period of time hopefully decreasing the stress experienced.

3.7.2. Results

After sintering had taken place the tubes were removed from the furnace, it was clear firstly that the tubes containing flour PFA had sintered most successfully with all 6 tubes remaining in one piece. Tubes made with flour PFA can be seen un-sintered in Fig.35. and the sintered tubes in Fig.36. there has been some movement due to shrinkage of the tubes during sintering mainly the un-milled tubes on the left hand side.

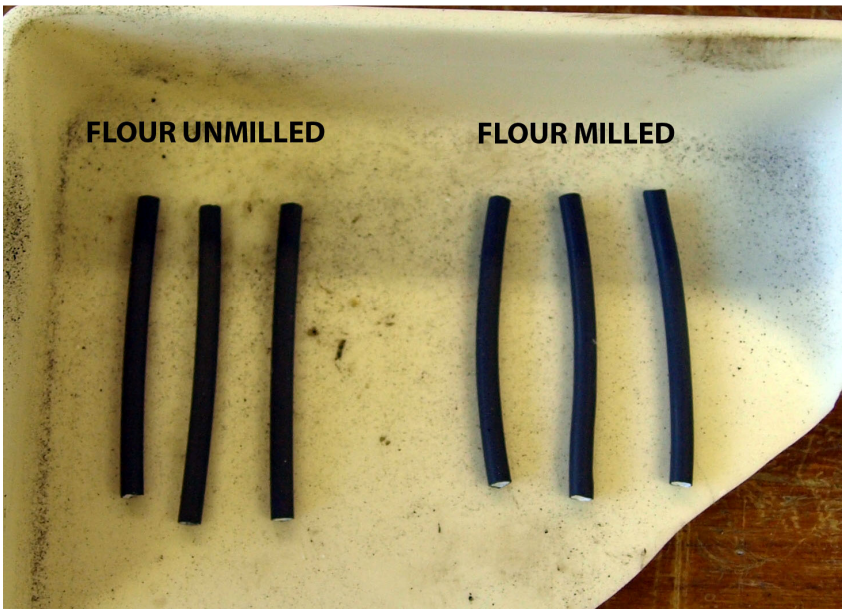

Fig.35. Un-sintered tubes containing flour PFA

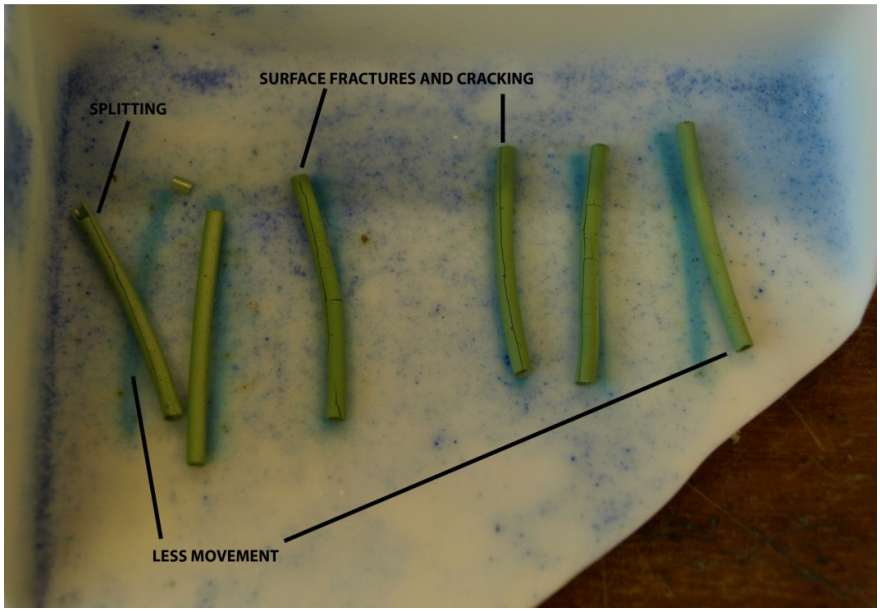

Fig.36. Sintered tubes containing flour PFA

Whilst these tubes performed better than both the carbon and the graphite containing tubes which can be seen below, there are still visible cracks on the surface of the tubes and in some places completely through the wall of the tube. Visually and by moving the tubes

with a metal spatula the tubes formed using milled powder had less surface defects and were structurally slightly more sound than the tubes formed using un-milled powders.

The un-sintered tubes containing graphite and carbon PFAs can be seen in Fig.37. and the sintered tubes in Fig.38. Firstly when compared to tubes containing flour PFA there can clearly be seen to have been a lot more movement of the tubes during sintering with several tubes appearing to have “exploded” during the sintering process. On first appearances the tubes containing carbon PFA which can be seen in the top of the picture appear to have suffered more during the sintering process than the tubes containing graphite PFA, suffering from more fractures, cracks and more movement. However between the large cracks where the tubes have completely failed there are less surface cracks and defects than in the graphite tubes.

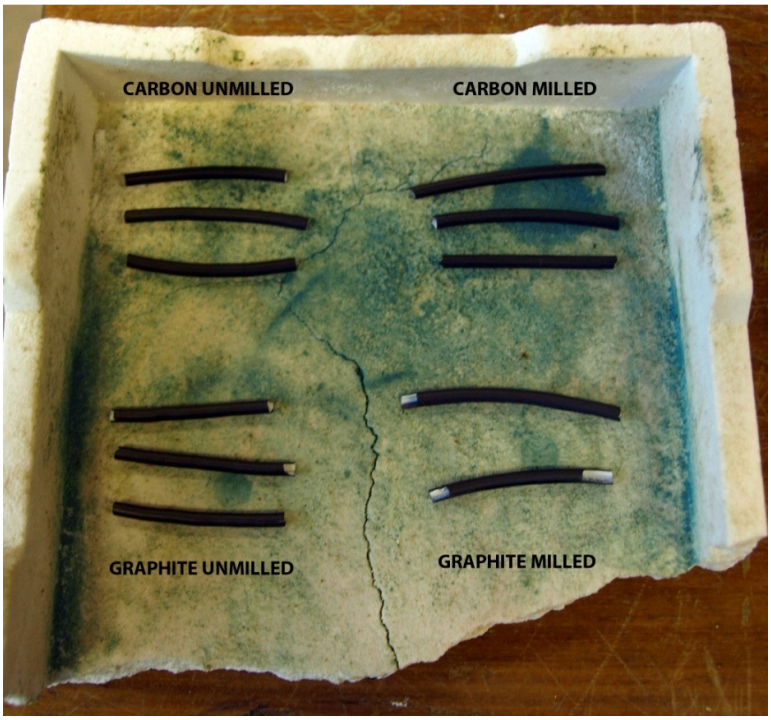

Fig.37. Un-sintered tubes containing carbon PFA and graphite PFA

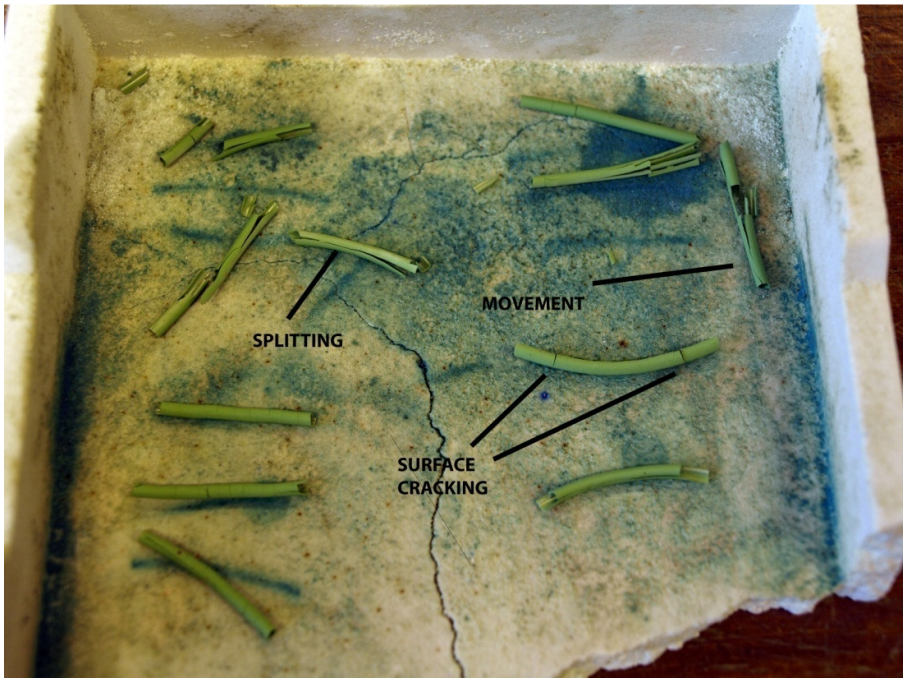

Fig.38. Sintered tubes containing carbon PFA and graphite PFA

As with the flour tubes, both sets of tubes were moved using a metal stirrer, this highlighted the fragility of the tubes with the graphite tubes all failing with very minimal force applied. The tubes containing carbon PFA also failed with minimal force, however they were marginally stronger than those made using graphite as the PFA.

The defects and the fragility of the tubes were not expected as the sintering programme took place over a longer period of time than the test samples which should have reduced the stress experienced due to the differences in thermal expansion of the materials as they would have expanded slowly over a greater period of time. The first test run may have been an anomalous result, in order to verify this a second set of tubes were run on the original sintering programme.

When a second set of carbon tubes were ran on the original shorter sintering programme, they were seen to split in a similar manner, but suffered from more surface fracture than those which were sintered over a longer period. Fig.39. shows the tubes after sintering and

it can be seen when compared to Fig.38. that they have suffered similar amounts of major cracking and splitting, however they had more surface defects and cracks which did not go through both layers of material. This is what would have been expected as due to the decreased time the expansions of the materials have happened quicker and caused more stress and therefore more cracking and splitting of the tubes.

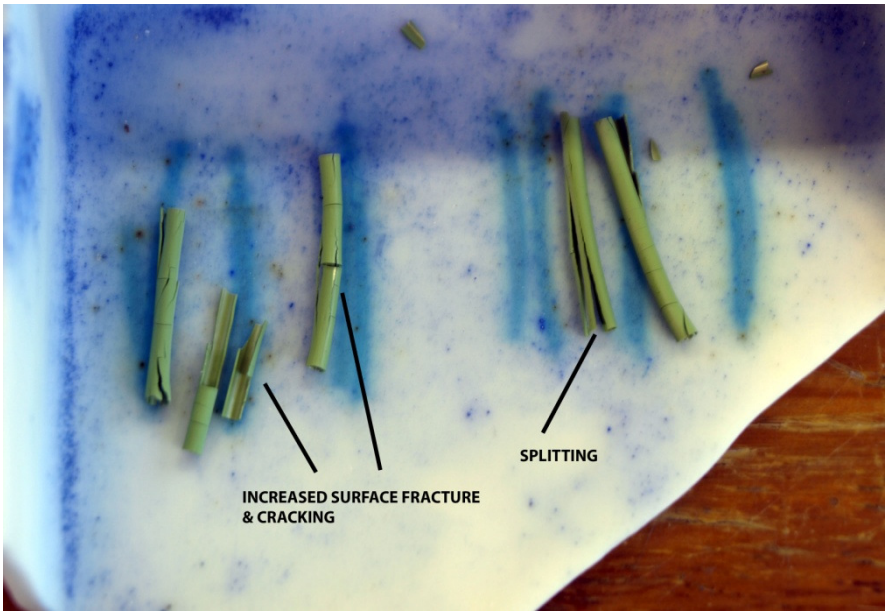

Fig.39. Sintered tubes containing carbon PFA

The sintering process once again highlighted issues using graphite as a PFA, having large amounts of surface defects as well as being difficult to extrude adding to the issues of paste forming. It was now seen that the sintered tubes were of too fragile to be used in any manufacturing situation. Tubes made using carbon as a PFA were also seen to be too fragile for use after sintering, this may have been due to the sintering programme, however a more likely explanation was the difference in thermal expansions and lack of intermediate layers of material.

Tubes made using flour as a PFA were seen to be strong enough to use within manufacture of an SOFC anode, however would be unsuitable for use due to the amount of surface

fracture and splitting seen. Again this issue could be overcome by the use of intermediate layers of material with smaller differences in thermal expansions which should lead to less cracking.

After sintering tubes were seen to have suffered from significant shrinkage, this was measured to be around 26% diametral shrinkage of the tubes. There was also a 20% shrinkage in the wall thickness after sintering.

3.8. Surface analysis

3.8.1. Method

All analysis of samples was carried out using a Philips XL30 ESEM scanning electron microscope at 10 kV, all samples were vacuum formed within an epoxy resin and then highly polished before analysis. This was done due to the fragility and difficulty of mounting the tubes in the correct orientation. After polishing the samples were sputter coated in carbon, this lead to large amounts of "charging" interference when viewed in the SEM due to electrons being retained in the sample rather than being transferred to the ground. To alleviate this all samples were sputter coated in gold which increased the conductivity and reduced the "charging" effect seen previously.

Imaging was carried out using secondary electron imaging, however due to the method of mounting in resin and then being polished secondary imaging was seen to be ineffective due to the smooth surface of the samples. To remedy this back scattered electron imaging was used to detect the difference between areas of different chemical composition which will allow for the different materials and pores to be identified more clearly.

3.8.2. EDX analysis

To identify which materials were seen on screen electronic dispersive x-ray analysis (EDX) was carried out on an area of the sintered tube containing carbon PFA. Fig.40. shows the analysis from one area, which shows that the light grey areas are NiO. Fig.41. shows the analysis for the darker areas, with large peaks visible for platinum and gold, the gold peak was expected as the sample was sputter coated in gold, the platinum peak is simply masking the zirconium peak, there are also carbon and nickel peaks, these areas are resin impregnated porous areas. Areas of pure YSZ are shown as almost white, these darker grey areas are actually pores containing YSZ NiO porous 3d skeletal structures.

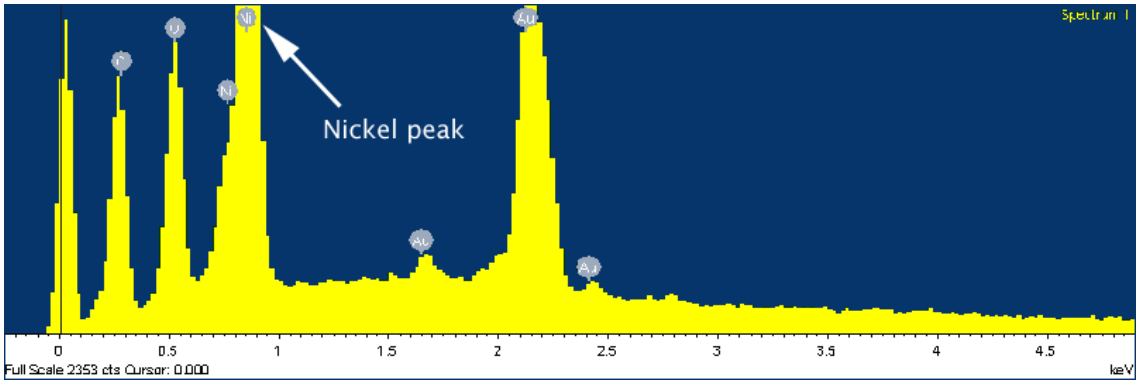

Fig.40. EDX analysis showing nickel peak (NiO)

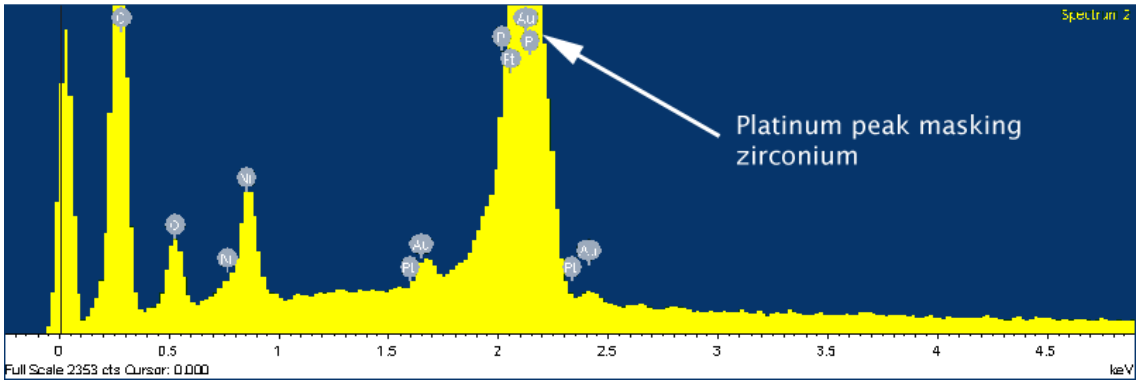

Fig.41. EDX analysis showing platinum peak masking zirconium (YSZ)

3.8.3. Carbon PFA tubes

Firstly in Fig.42. the un-sintered tube micro-structure with un-milled powders containing carbon PFA can be seen, the pure YSZ particles can be seen on the far left hand of the image, with the NiO YSZ carbon mixture on the right. From the image the particles appear to be reasonably well distributed however there are clearly visible areas where NiO has agglomerated together with the carbon and YSZ particles mixed together around these areas.

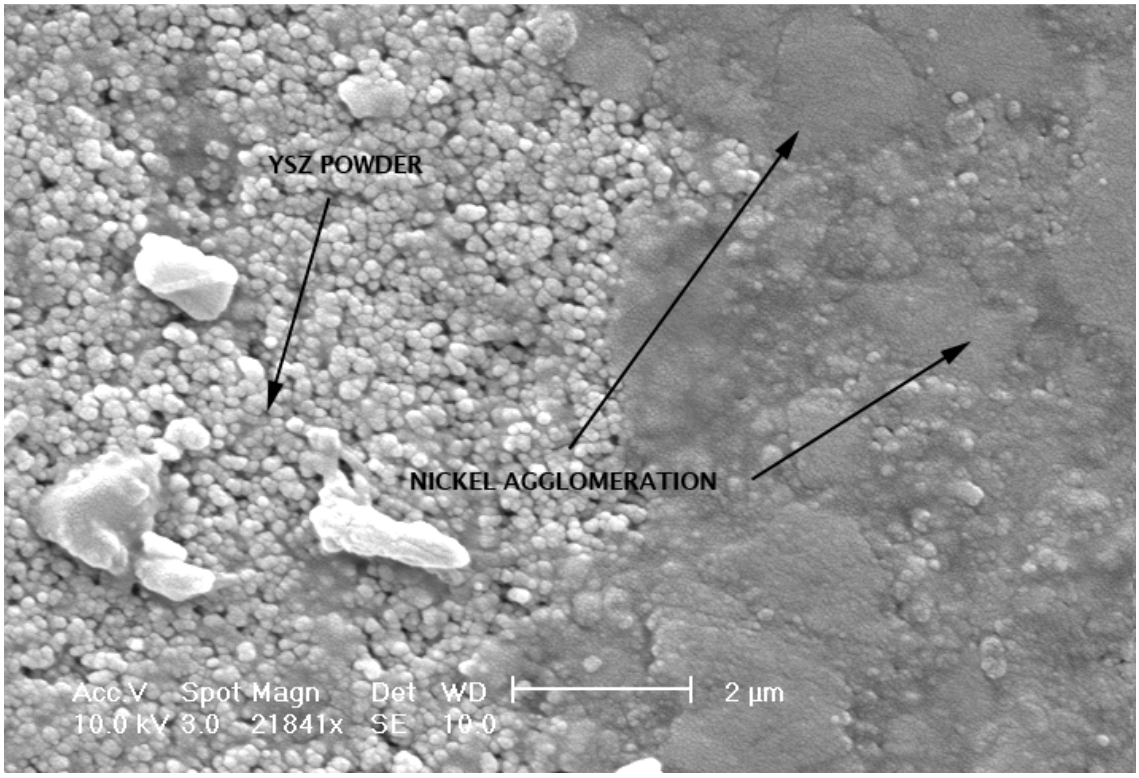

Fig.42. SEM image of un-sintered tube with un-milled powders containing carbon PFA

Fig.43. shows the un-sintered tube micro-structure with milled powders containing carbon PFA with the YSZ particles on the right hand side of the image and the NiO YSZ carbon mixture on the left. When compared to Fig.42. there are still the agglomerated areas of NiO with the carbon and YSZ in the surrounding areas, however these agglomerates

appear to be more frequent in number yet reduced in size. The surrounding area of carbon and YSZ appears to be more uniform suggested by the more uniform colour, this would suggest better mixing of the particles.

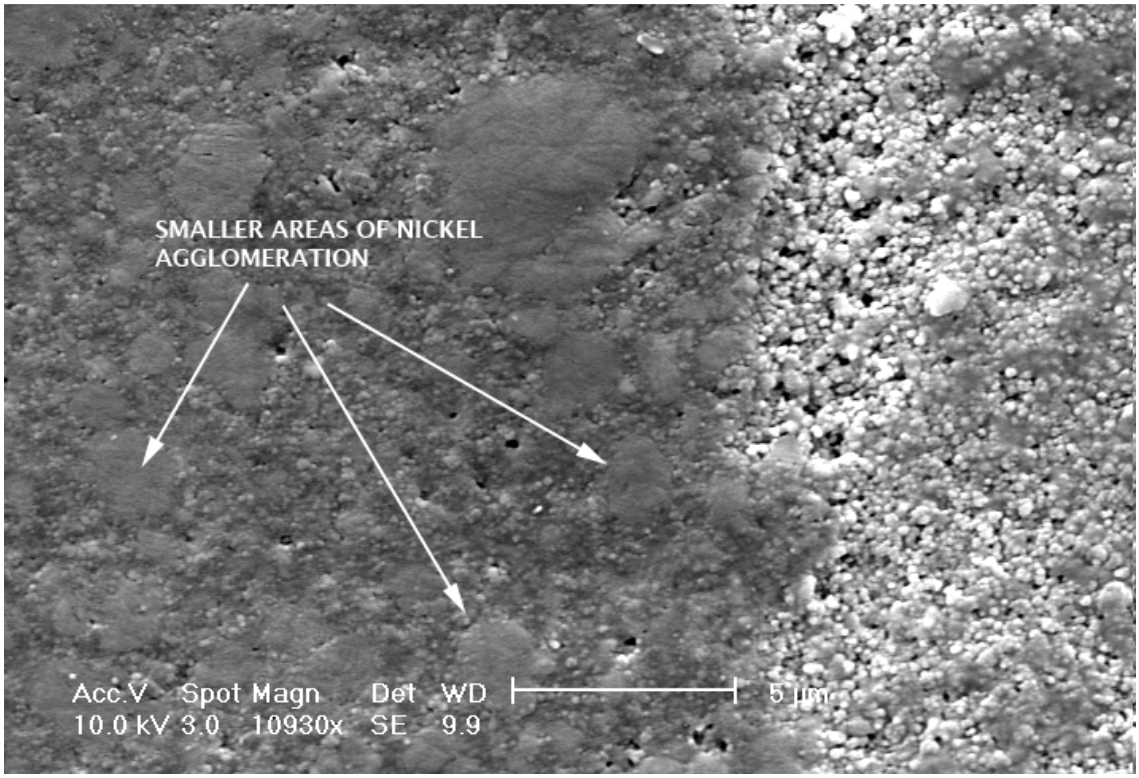

Fig.43. SEM image of un-sintered tube with milled powders containing carbon PFA

In Fig.44. the sintered tube micro structure with un-milled powders containing carbon PFA can be seen as stated previously from EDX analysis the lighter areas are NiO with some small bits of YSZ, the darker grey areas are pores containing skeletal YSZ NiO structures impregnated with epoxy resin and the black areas are pure pores. There can be seen to be large areas of solid nickel with no porosity, this is due to the agglomeration of NiO seen in Fig.42. and also due to issues with nickel oxide grain growth at high temperatures. Pores can be seen to be relatively well distributed, however small in size, typically a few microns in cross section.

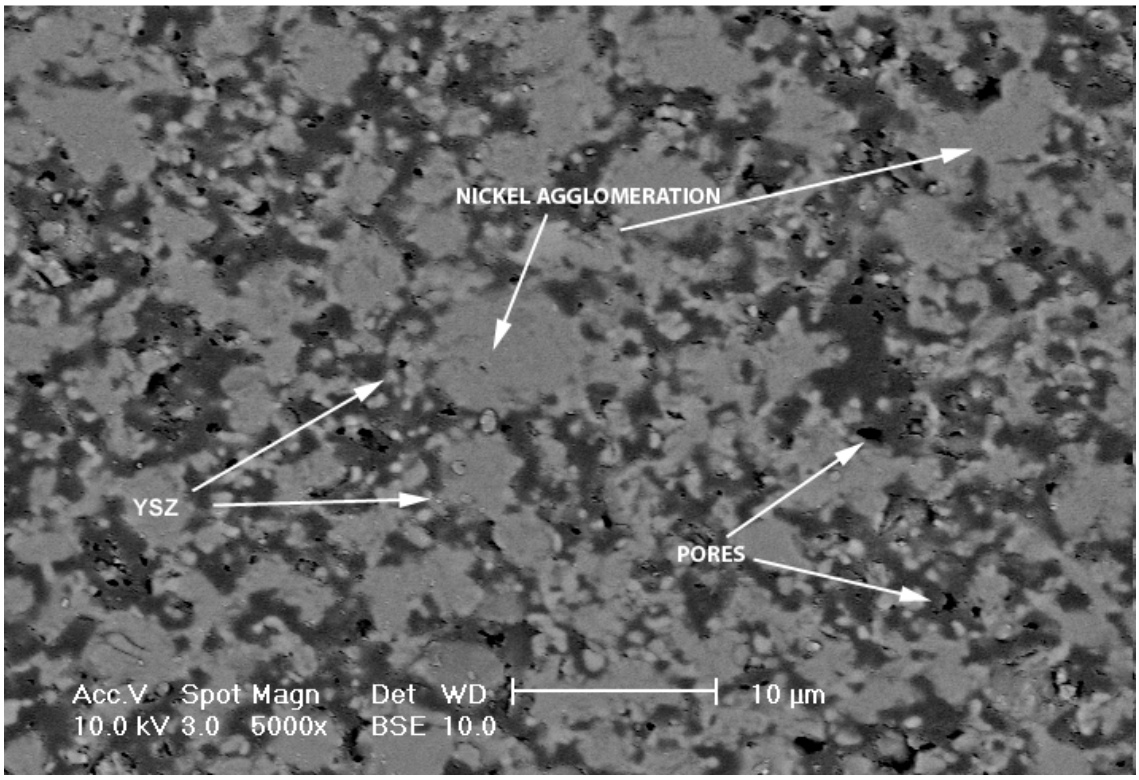

Fig.44. SEM image of sintered tube with un-milled powders containing carbon PFA

In Fig.45. the sintered tube micro-structure with milled powders containing carbon PFA can be seen, firstly when compared to Fig.44. there can be seen to be a better overall distribution of pores NiO and YSZ. However as seen in Fig.44. there were still large areas of solid NiO, these are smaller than those seen in the un-milled sample however due to the nature of nickel grain growth at high temperatures they are still present. Despite the nickel oxide grain growth issues there can be seen to be a better distribution of the NiO through the micro-structure of the sample.

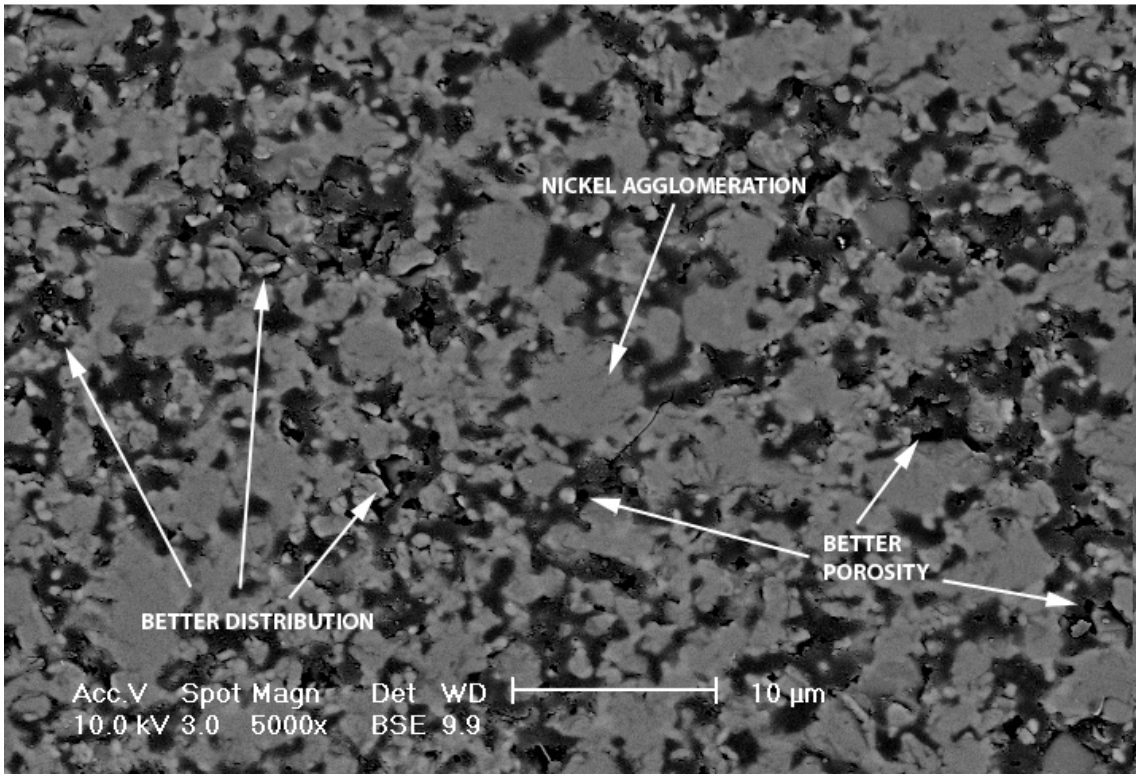

Fig.45. SEM image of sintered tube with milled powders containing carbon PFA

There was seen to be a similar amount of darker grey areas containing porosity however were more visible black pores within the sample, being better distributed, more numerous and greater in size than those seen in Fig.44. This illustrates that the sample had a better skeletal formation with better porosity, this was the expected result as the milling of the powders prior to paste preparation and sintering should have lead to a better mixed and more uniform powder than the un-milled sample.

3.8.4. Graphite PFA tubes

As seen with the tubes containing carbon PFA, milling was seen to better distribute PFA particles within the tubes containing graphite PFA. Fig.46. shows the un-sintered tube micro-structure with un-milled powders containing graphite PFA, with few dark graphite particles visible, Fig.47. shows the un-sintered tube micro-structure with milled powders containing graphite PFA and it can be seen that there were fewer large graphite particles and generally particles better distributed throughout the micro-structure.

The sintered tube micro-structure with un-milled powders containing graphite PFA can be seen in Fig.48. again issues with nickel oxide grain growth can be seen with large areas of non porous NiO visible over the micro-structure. There were very few unfilled pores visible over the micro-structure, those that were visible were very small in size, there was a significant amount of darker porous areas however surrounding the NiO YSZ composite.

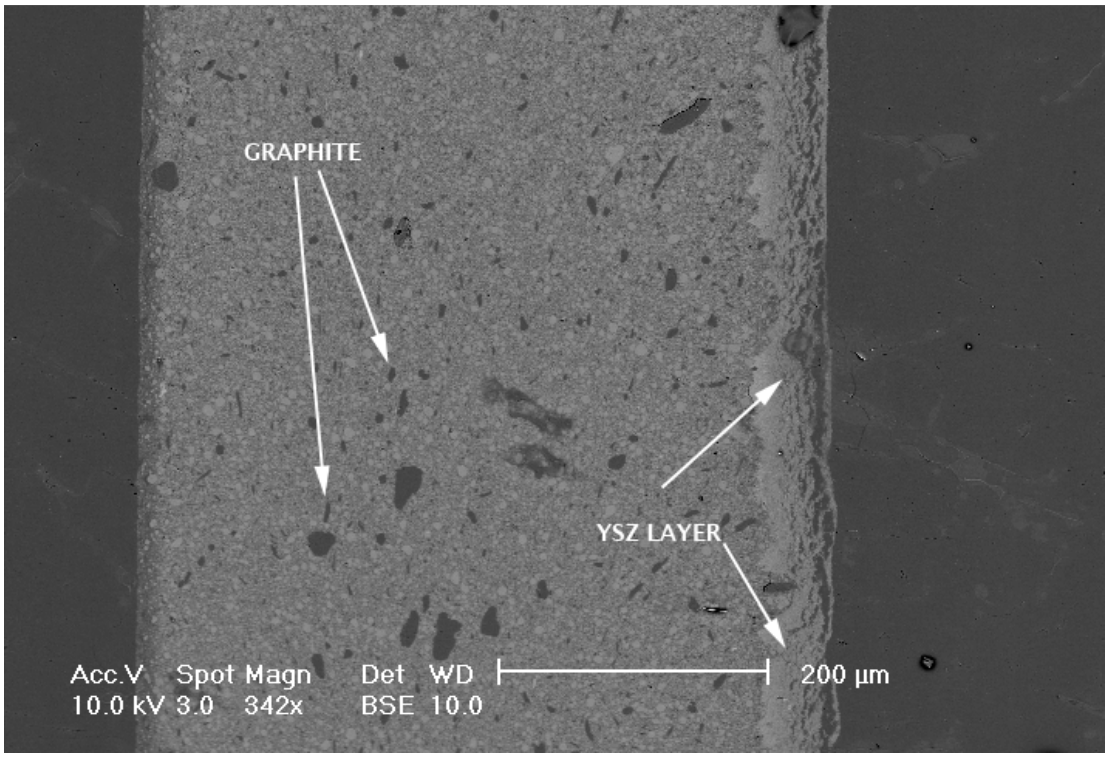

Fig.46. SEM image of un-sintered tube with un-milled powders containing graphite PFA

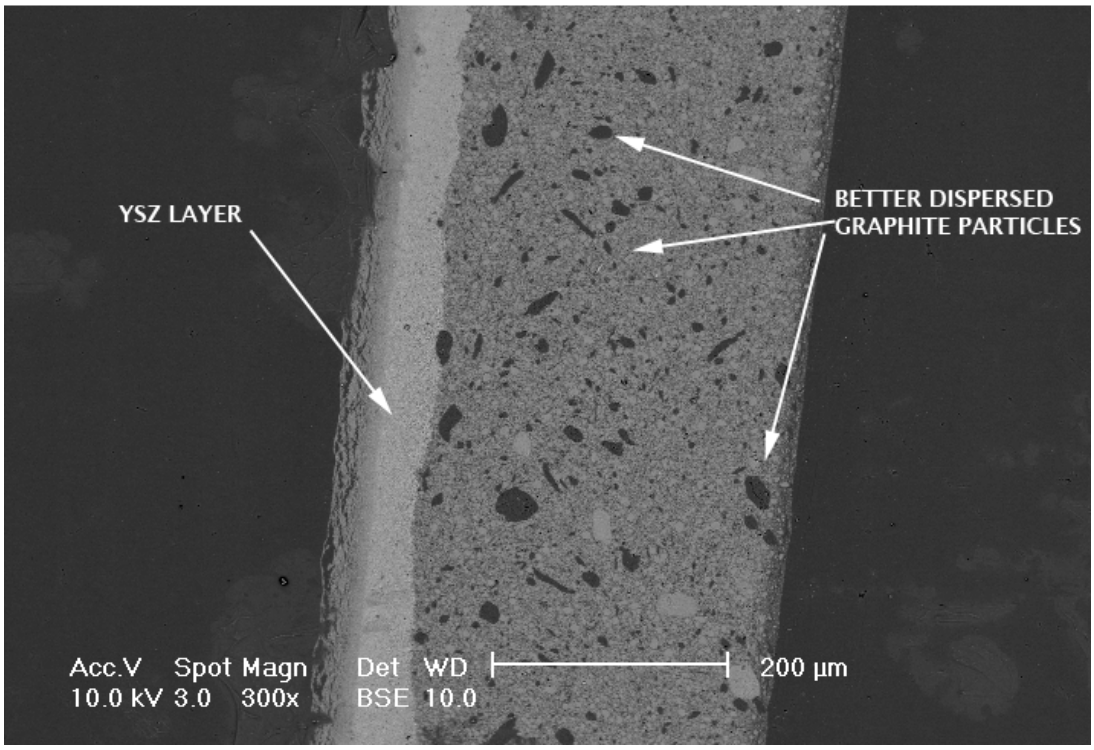

Fig.47. SEM image of un-sintered tube with milled powders containing graphite PFA

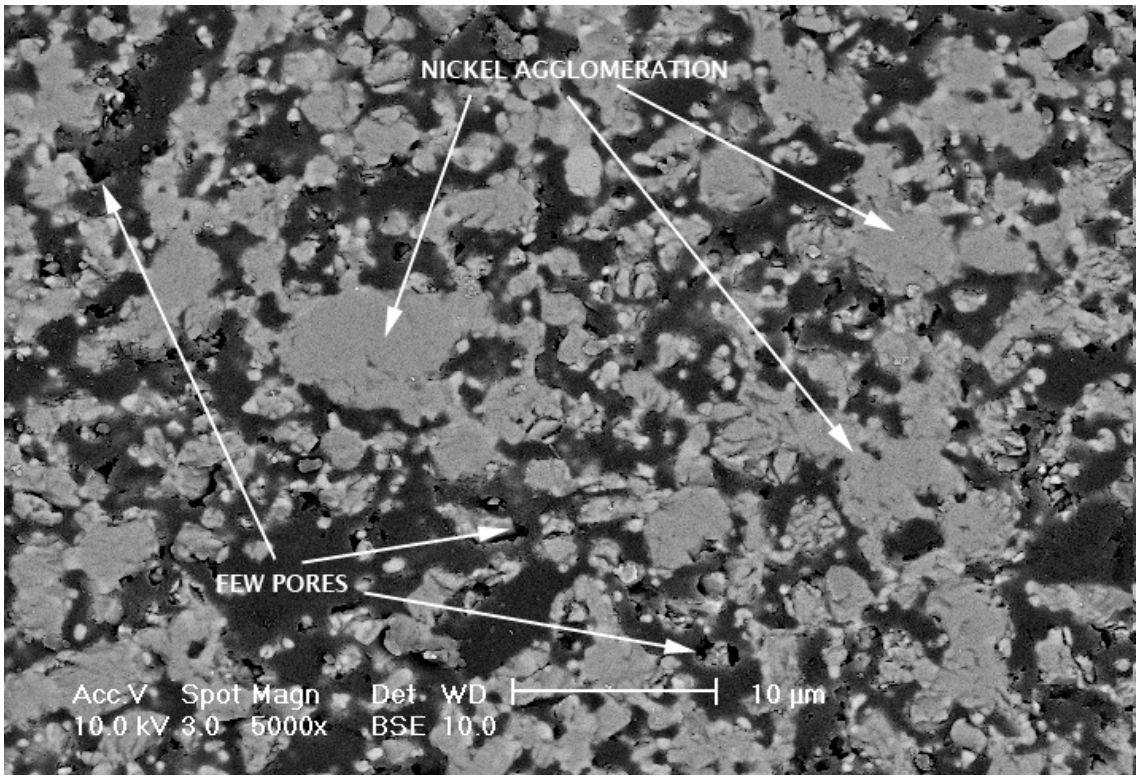

Fig.48. SEM image of sintered tube with un-milled powders containing graphite PFA

Fig.49. shows the sintered tube micro-structure with milled powders containing graphite PFA, nickel oxide grain growth again is clearly visible, however unlike the carbon tubes there appeared to be very little if any improvement in the agglomeration of NiO in the milled powder tube compared to the un-milled powder tube. The overall porosity of the tube appears to be similar to the un-milled powder tube but with an increase in the number and size of pure black pores, indicating a finer pore structure preventing resin impregnation. White YSZ particles can also be seen across the micro-structure in particular within the larger porous areas with exposed skeletal structure.

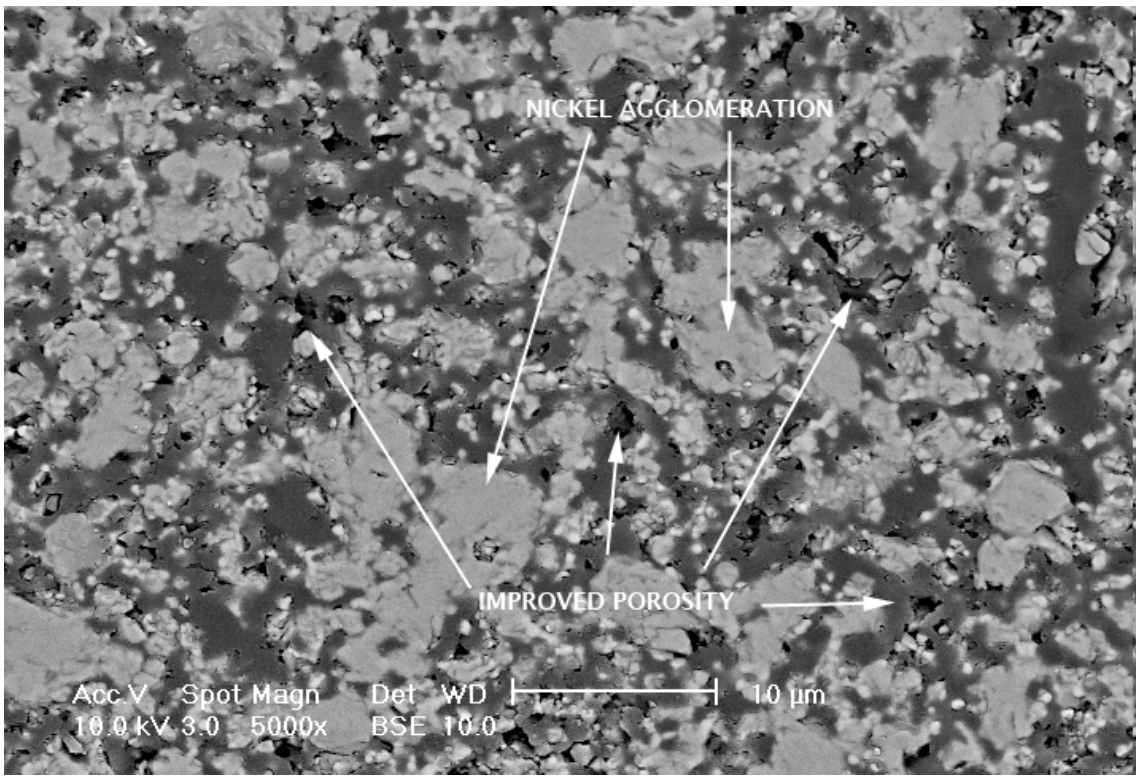

Fig.49. SEM image of sintered tube with milled powders containing graphite PFA

3.8.5. Flour PFA tubes

The un-sintered tube micro-structure with un-milled powders containing flour PFA is shown in Fig.50., there can be seen to be very few non impregnated pores over the surface, however the pores present can be seen to be very large in size. These large pores were likely caused due to air trapped within the system during the extrusion process. There are few areas of flour particles that are fairly well distributed over the micro-structure.

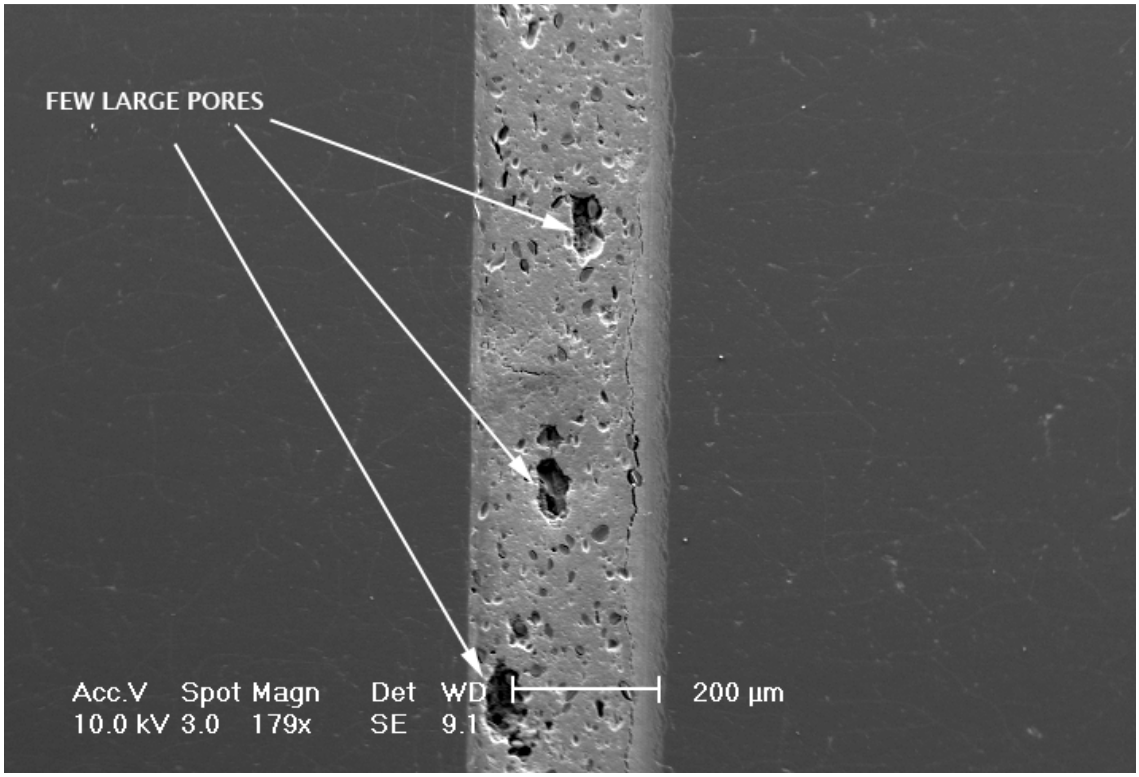

Fig.50. SEM image of un-sintered tube with un-milled powders containing flour PFA

In Fig.51. the un-sintered tube micro-structure with milled powders containing flour PFA is seen, the milling has improved the number of pores over the micro-structure of the tube, with greater numbers of smaller pores visible. The distribution of the flour was also improved with again greater numbers of smaller areas of flour seen over the whole micro-structure.

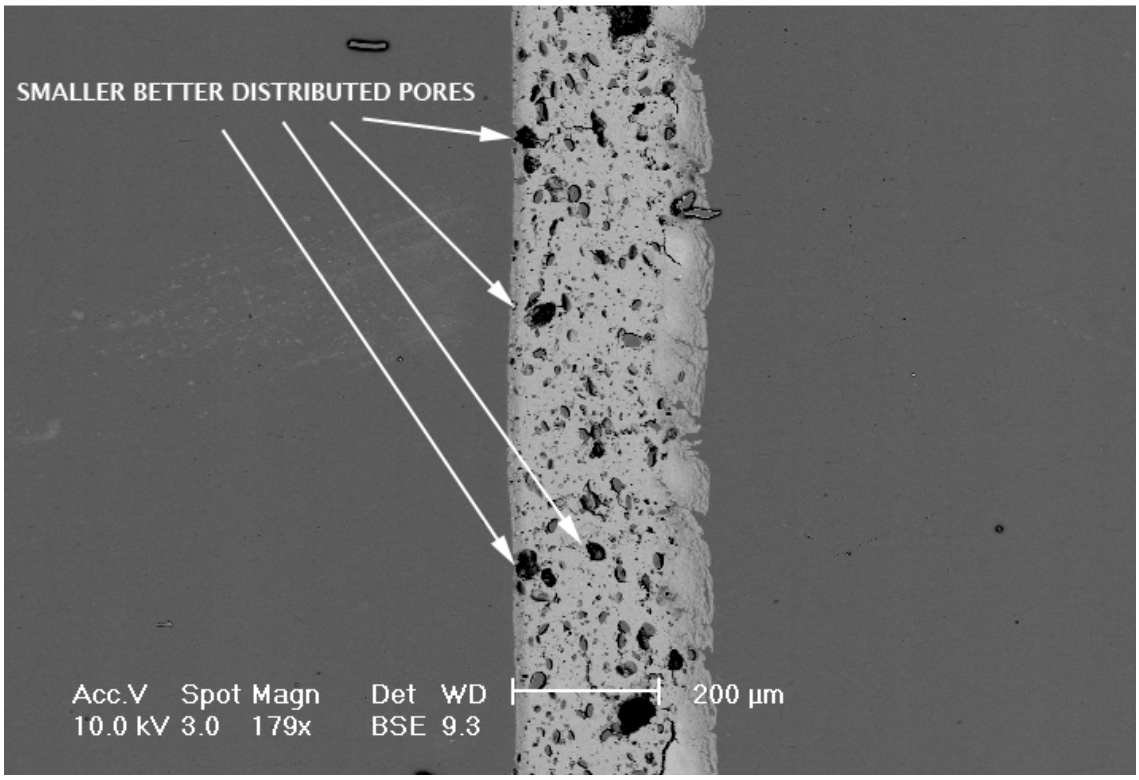

Fig.51. SEM image of un-sintered tube with milled powders containing flour PFA

BSE imaging was used for all samples due to the smoothness of the surface after polishing during mounting of samples, however the structure of the tubes containing flour PFA were seen to be porous with a skeletal structure visible using SE imaging instead. Fig.52. shows the sintered tube micro-structure with un-milled powders containing flour PFA, firstly it was observed that there were few pure pores with limited porosity over the micro-structure. Significant amounts of nickel oxide grain growth were observed with most of the micro-structure appearing to consist of non porous NiO areas YSZ was non identifiable.

Fig.53. shows the sintered tube micro-structure with milled powders containing flour PFA, there were still clearly large areas of nickel oxide agglomeration over the micro-structure. There was also much better visible porosity along with large pure pores, within these large pores it was possible to see the skeletal structure of the tube micro-structure, showing an improvement over then un-milled tube containing flour PFA.

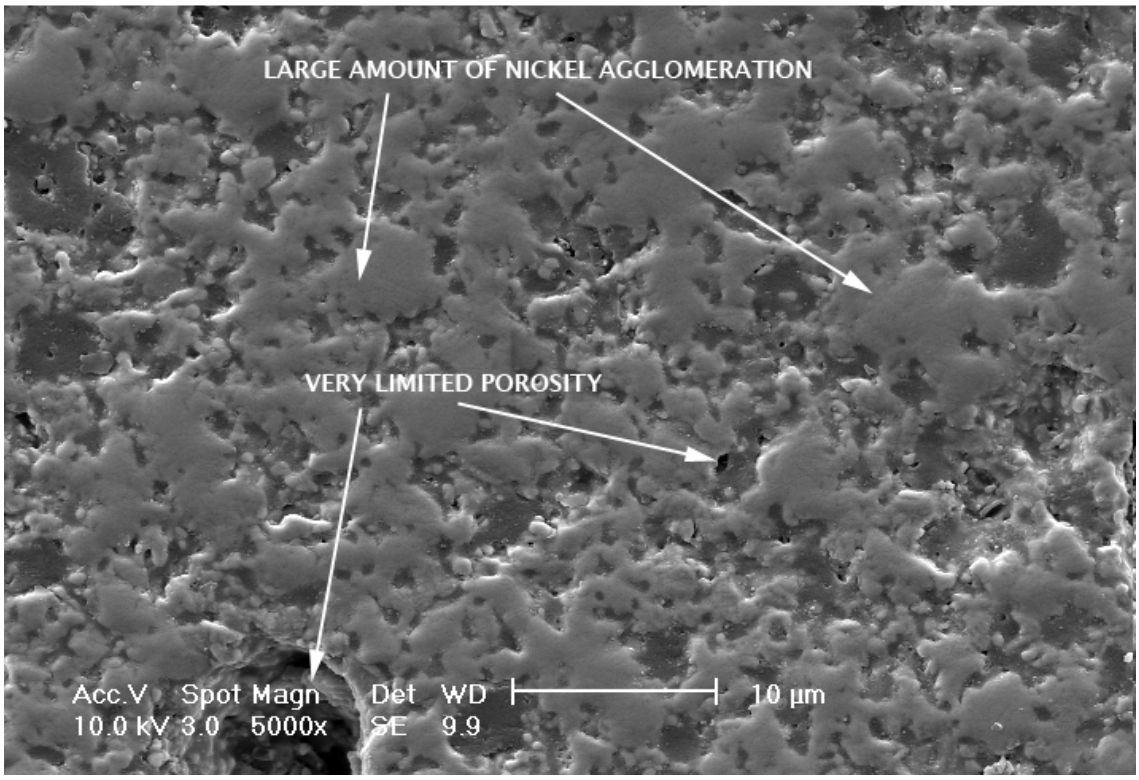

Fig.52. SEM image of sintered tube with un-milled powders containing flour PFA

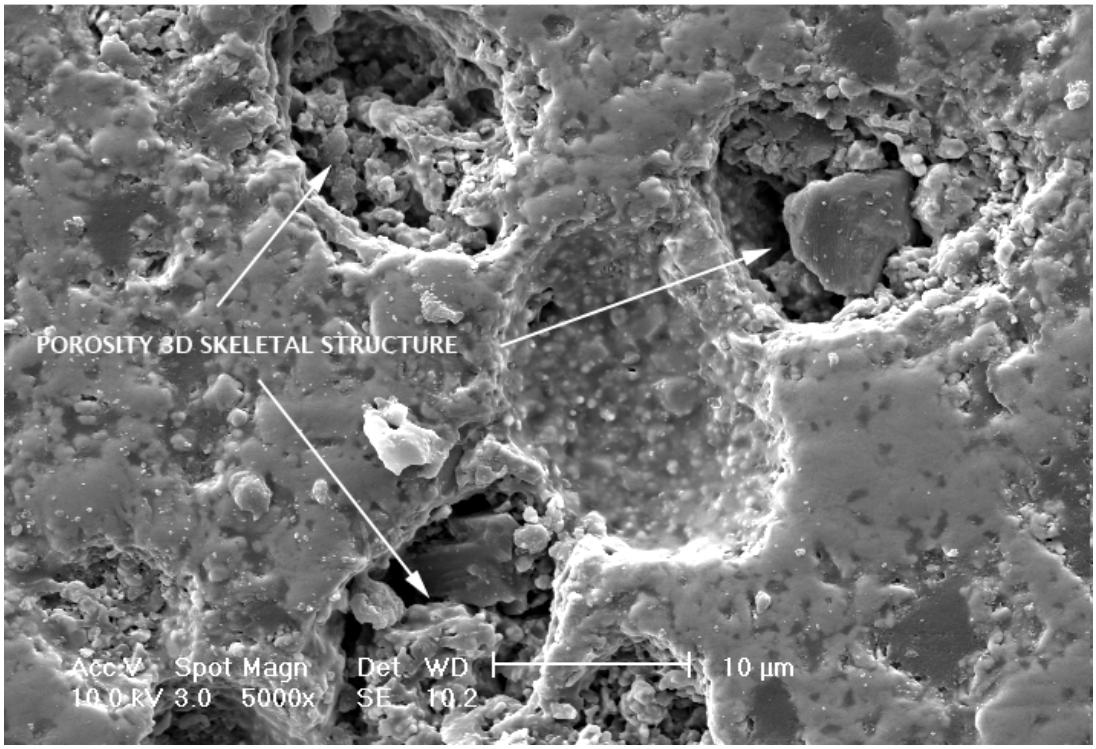

Fig.53. SEM image of sintered tube with milled powders containing flour PFA

3.8.6. PFA comparison

All samples showed improvements in both porosity and dispersion of NiO throughout their respective micro-structures when comparing milled to un-milled powders. This was expected as the milled powders had undergone more intense mixing and particle size refinement before paste processing and sintering.

Out of the three PFAs investigated graphite and carbon as seen in Fig.54. and Fig.55. respectively offered similar microstructures with small pores ~10 μm shown to be well distributed across the whole tube micro-structure. The solid pale area showing the solid non porous YSZ paste, the darker area showing the YSZ NiO cermet, and the small black areas showing the most porous areas over the micro-structure.

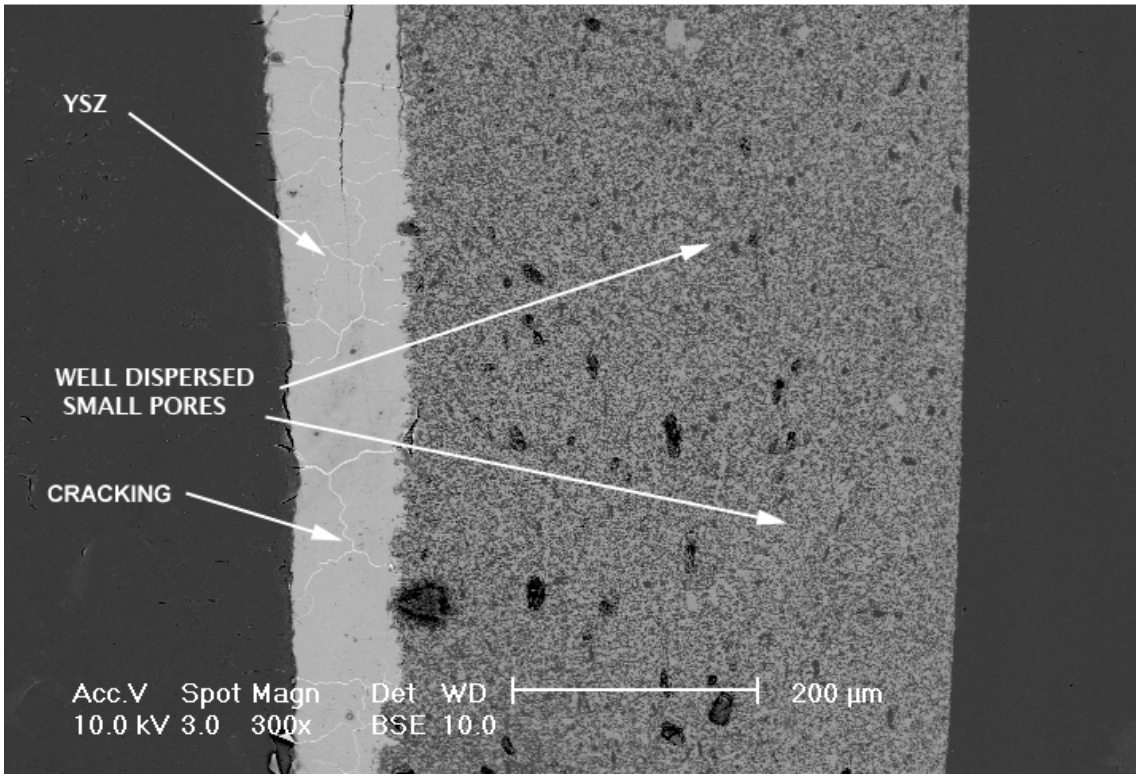

Fig.54. SEM image of sintered tube with milled powders containing graphite PFA

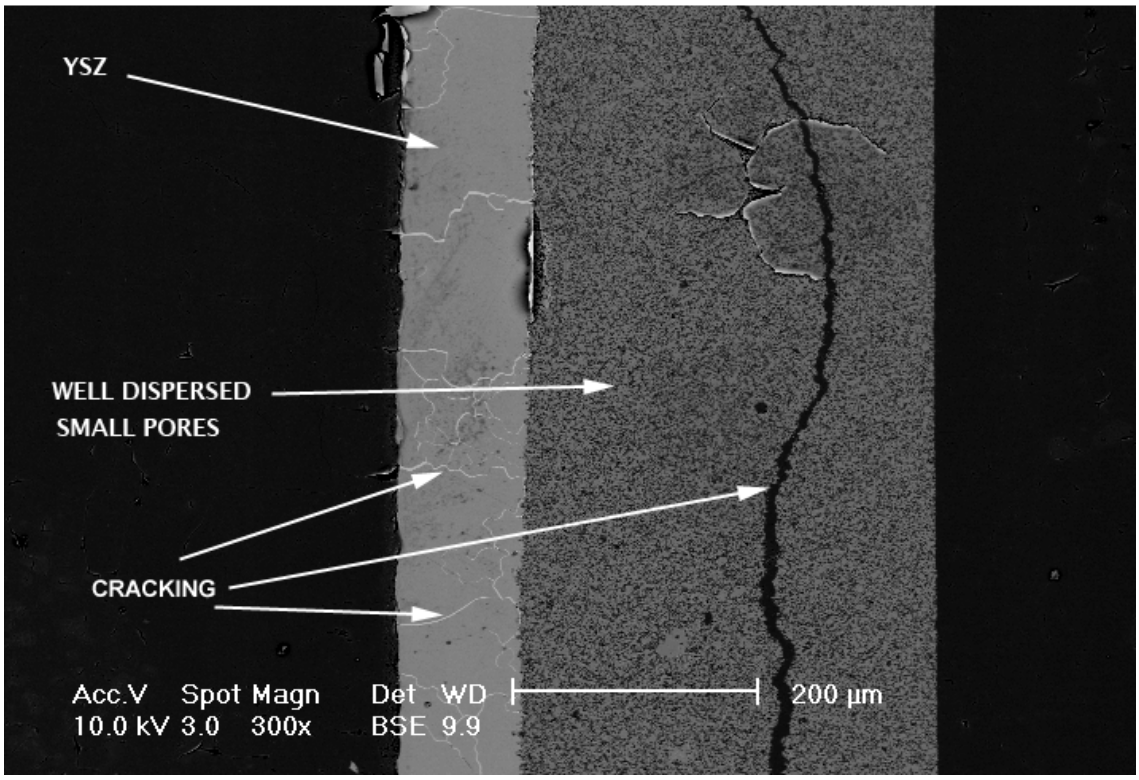

Fig.55. SEM image of sintered tube with milled powders containing carbon PFA

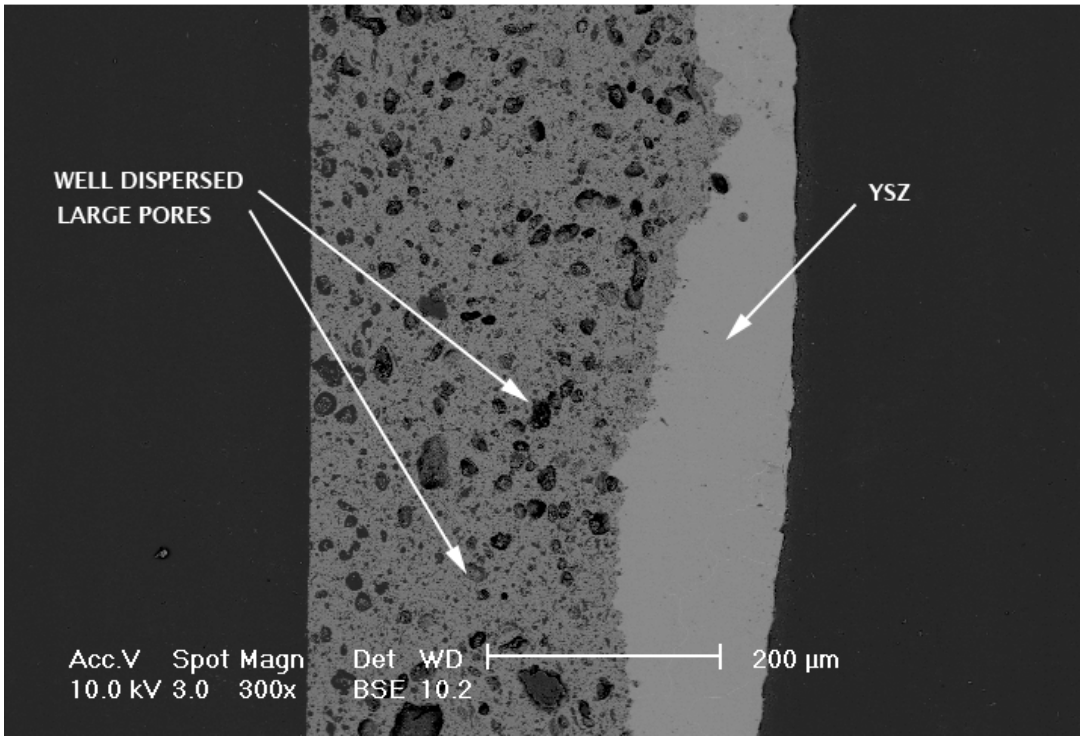

Fig.56. SEM image of sintered tube with milled powders containing flour PFA

The tube containing milled powders with flour PFA was seen to have larger well dispersed pores over its micro-structure as shown in Fig.56. The flour PFA also had a better more clearly visible three dimensional skeletal structure as shown in Fig.53. this suggests the flour to be the best performing PFA as this porous skeletal structure would lead to the system containing the largest number of TBPs during SOFC operation.

Throughout analysis issues due to cracking primarily within the pure YSZ electrolyte layer were visible, as shown in Fig.54. and Fig.55. This cracking was due to differences in thermal expansion co-efficients between layers and would produce a tube unsuitable for use within an SOFC. This was seen within the tubes containing both graphite and carbon PFAs but not within tubes containing flour PFA as shown in Fig.56. suggesting that flour offers the best PFA solution from a structural view point

4. CONCLUSIONS

4.1. Porosity forming agent (PFA)

The suitability of materials for use as PFA was investigated by means of pellet sintering. Four candidate materials namely graphite, carbon black, potato starch and wheat flour were sintered initially. After sintering was completed and PFA material had been pyrolised it was observed that graphite, carbon black and wheat flour were suitable for this application and were further investigated. Potato starch was seen to perform very poorly and as such was discarded as a suitable PFA and not investigated further.

4.2. Milling

It was observed that three minutes of TEMA milling was sufficient to reduce the average particle size seen of all powders to 3.38 μm in size from 12.8 μm. After milling particle size distribution was reduced with 100% of particles passing 10 μm where as previously only 54.1% passed 10 μm.

4.3. Paste preparation

During the processing of the pastes it was observed that those containing milled constituent powders mixed to form a homogenous paste faster than those with un-milled powders. Of the three PFA powders investigate graphite proved hardest to form into a usable paste.

4.4. Tube extrusion

All pastes extruded successfully through the die system under the 30 kN load limit. Pastes containing flour PFA were observed to extrude at the lowest force (11.4 kN), with graphite requiring the most force to extrude successfully (15.2 kN). It was also observed that pastes

containing milled powders extruded at lower forces than those pastes containing un-milled powders. Again issues with graphite as a PFA were noticed, with large surface defects observed in the graphite PFA tubes, along with large amounts of wasted pastes due to difficulties to form tubes at all.

4.5. Tube sintering

After sintering large amounts of surface fracture and cracking were visible universally over all samples regardless of PFA or milling. This was due to the large difference in thermal expansion co-efficients between the two layers of different material in each tube.

From the three PFAs investigated tubes formed using carbon and graphite were seen to be much more fragile than those containing flour. After sintering tubes derived with flour PFA appeared to offer the best performance of the PFAs tested in terms of structural strength of the resultant tubes. It was not possible to establish the influence of milling on the structural strength as all tubes were too fragile for testing to be conducted.

4.6. Surface & microstructure analysis

SEM analysis established that milling of constituent powders before mixing and processing into pastes led to a better distribution of NiO over the surface and throughout the micro-structure of the tubes. Improvements in the size, number and distribution of pores were also observed in pastes containing milled powders of all investigated PFAs.

Graphite as an alternative PFA achieved similar levels of distribution and porosity to that of carbon and as such showed no advantages as an alternative PFA. Analysis of tubes containing flour showed much larger pores, with a better skeletal structure clearly visible when compared to the original carbon PFA, suggesting that flour offered the best PFA solution out of the materials investigated. Additionally the compatibility of the co-extruded

materials was shown by the reduced amount of cracking visible within the YSZ electrolyte layer compared to tubes formed using graphite or carbon PFA.

The best solution to improvement of porosity and dispersion of nickel oxide over the surface and throughout the micro-structure of SOFC anode tubes found within this investigation was using flour as the PFA. Combined with processing of powders for three minutes with a TEMA mill before paste processing and sintering.

5. FUTURE WORK

5.1. Powder processing / milling

The aim of this investigation was to improve the distribution of NiO and pores over the surface and throughout the micro-structure of an SOFC anode. This was achieved using a TEMA mill, however alternative methods of milling were not investigated. While this milling achieved some level of success in improving dispersion there were still issues with the sintered tubes.

The issue of nickel grain growth was still found to be prevalent after the milling employed within this investigation, this is due to the high sintering temperature required in the manufacture of the tubes. Grain growth can be reduced by lowering the sintering temperature, milling of powders can lead to a reduction in the sintering temperature required.

A further study of the effect of milling and the subsequent lowering of the sintering temperature required would establish by how much the sintering temperature could be reduced when compared to milling processing times. Also the economical factor of whether the increased cost and time during processing of powders could be recouped by the reduction of the sintering temperature and processing times of pastes should be studied.

During this investigation NiO, YSZ and PFA powders were milled together. The effects of milling just the NiO and YSZ powders whilst leaving the PFA powder as received could also be investigated. This should allow for more NiO YSZ powder interactions allowing for a reduction in sintering temperature but leaving the PFA with larger sized particles to form larger pores within the sintered surface and micro-structure.

5.2. Porosity forming agent (PFA)

During this investigation several PFAs were investigated with wheat flour appearing to produce the best and most desired properties in the sintered SOFC tube. However as discussed previously due to the time constraints within this investigation only two layers were used to create the tube which lead to unwanted surface fracture and cracking.

To establish better the effectiveness of flour as a PFA more intermediate layers between the pure YSZ electrolyte layer and the 80% NiO anode layer should be investigated. These intermediate layers should reduce the stress experienced due to the varying thermal expansions, leaving a surface that is less cracked and allowing the properties of flour as a PFA to be fully established.

6. REFERENCES

[1] S. K. Park, K. S. Oh, T. S. Kim, Journal of Power Sources 170 (2007) 130-139.

[2] S. C. Singhal and K. Kendall, Introduction & History, in: High Temperature Solid Oxide Fuel Cells, (2004) 1-53

[3] W. Nernst, Z. Electrochem., 6 (1899) 41.

[4] E. Baur and H. Preis, Z. Electrochem., 43 (1937) 272.

[5] P. Reichner and J. M. Makiel, Development Status of Multi-cell Solid Oxide Fuel Cell Generators, 1986 National Fuel Cell Seminar Abstracts, Washington DC, (1982) 32-35

[6] J. T. Brown, Solid Oxide Fuel Cells, High Conductivity Solid Ionic Conductors, World Scientific, (1989) 630-663

[7] http://www1.eere.energy.gov/hydrogenandfuelcells/fuelcells/fc_types.html , accessed March 2009.

[8] A. O. Isenberg, Solid State Ionics, 3 (1981) 431.

[9] C. Bagger, Improved Production Methods for YSZ Electrolyte and Ni-YSZ Anode for SOFC, Fuel Cell Seminar Abstracts, Tuscon AZ, (1992)

[10] J. Powell, The Development of a Process for The Manufacture of Multilayered Ceramic Micro-tubes, University of Birmingham, (2008) 40-44

[11] K. C. Wincewicz, J. S. Cooper, Taxonomies of SOFC Material and Manufacturing Alternatives, Journal of Power Sources 140 (2005) 280-296.

[12] W. Bujalski, C. M. Dikwal, K. Kendall, Cycling of Three Solid Oxide Fuel Cell Types, Journal of Power Sources 171 (2007) 96-100.

[13] S. C. Singhal, Advances in Tubular Solid Oxide Fuel Cell Technology, 4th International Symposium on Solid Oxide Fuel Cells, (1995) 7-17.

[14] F. Haber and A. Moser, Z. Electrochem., 11 (1905) 593-609.

[15] H. Mobius, J. Solid State Electrochem., 1 (1997) Chapter 2.

[16] S. C. Singhal and K. Kendall, Anodes, in: High Temperature Solid Oxide Fuel Cells, (2004) 149-171.

[17] H. S. Spacil, US Patent 3,558,360; filed October 30, 1964, modified November 2, 1967, granted March 31, 1970.

[18] S-D. Kim, H. Moon, J. Moon, Nio-YSZ Composite Powder for High Performance and Durability of Solid Oxide Fuel Cells, Solid State Ionics 178 (2007) 1304–1309.

[19] C. Yang, W. Li, S. Zhang, L. Bi, R. Peng, C. Chen, Fabrication and Characterization of an Anode-Supported Hollow Fiber SOFC, Journal of Power Sources 187 (2009) 90–92.

[20] R.F. Martins, M.C. Brant, R.Z. Domingues, R.M. Paniago, K. Sapag, T. Matencio, Synthesis and characterization of NiO-YSZ for SOFCs, Materials Research Bulletin 44 (2009) 451–456.

[21] J. H. Yu, G.W. Park, S. Lee, S.K. Woo, Microstructural Effects on the Electrical and Mechanical Properties of Ni–YSZ Cermet for SOFC Anode, Journal of Power Sources, Volume 163, Issue 2, (2007) 926-932.

[22] J. Powell, The Development of a Process for The Manufacture of Multilayered Ceramic Micro-tubes, University of Birmingham, (2008) 40-44

[23] N Ai, Z. Lu, K. Chen, X. Huang, X. Du, W. Su, Effects of Anode Surface Modification on the Performance of Low Temperature SOFCs, Journal of Power Sources Volume 171, Issue 2, (2007) 489-494.

[24] E. Y. Gutmanas, Materials With Fine Microstructures by Advanced Powder Metallurgy, Progress in Materials Science, Volume 34, Issue 4, (1990) 261-366.

[25] G. E. Totten, L Xie, K. Funantani, Handbook of Mechanical Alloy Design, New York: M . Dekker, (2004)

[26] P. R. Soni, Mechanical Alloying: Fundamentals and Applications, Cambridge International Science Publishing, (2001)

[27] E. Artz, L. Shultz Eds, New Materials by Mechanical Alloying, Deutsche Geselschaft fur Metallkunde, Germany, (1989)

[28] J. Kübarsepp, Characterization of the Serviceability of Steel-Bonded Hardmetals, International Journal of Refractory Metals and Hard Materials, Volume 12, Issue 6, (1993-1994) 341-348

[29] S. Lee, J-M. Kim, H.S. Hong, S-K Woo, Fabrication and Characterization of Cu/YSZ Cermet High Temperature Electrolysis Cathode Material Prepared by High-energy Ball-milling Method II., Journal of Alloys and Compounds 467, (2009) 614–621.

[30] H. S. Hong, U-S. Chae, S-T. Choo, The Effect of Ball Milling Parameters and Ni Concentration on a YSZ-coated Ni Composite for a High Temperature Electrolysis Cathode, Journal of Alloys and Compounds, 449, (2008) 331–334.

[31] T. A. G. Restivo and S. R. H. D. Mello-Castanho, Nickel-Zirconia Cermet Processing by Mechanical Alloying for Solid Oxide Fuel Cell Anodes, Journal of Power Sources 185 (2008) 1262–1266.

[32] J. J. Benbow, J. Bridgwater, Paste Flow and Extrusion, Clarendon Press, Oxford, 1993.

[33] http://www.sweetthoughts.co.uk/acatalog/How is Rock Candy Made.html, accessed March 2009.

[34] Stuart Blackburn, D. Ian Wilson, Shaping ceramics by plastic processing, Journal of the European Ceramic Society 28 (2008) 1341–1351.

[35] Z. Chen, K. Ikeda, T. Murakami, T. Takeda, Journal of the American Ceramics Society 83 (2000) 1081-1086.

[36] C. Van Hoy, A. Barda, M. Griffith, J. W. Halloran, Journal of the American Ceramics Society 81 (1998) 152--158.

[37] Stuart Blackburn, Benobow Bridgwater demonstration, Birmingham University, 2009.

[38] A. D. U. S. Amarasinghe and D. I. Wilson, Interpretation of Paste Extrusion Data, Institution of Chemical Engineers,Trans IChemE, Vol 76, Part A, January 1998.

[39] M. Buckley, Dry processing of industrial minerals, PhD thesis, University of Birmingham, (2008).

7. APPENDIX

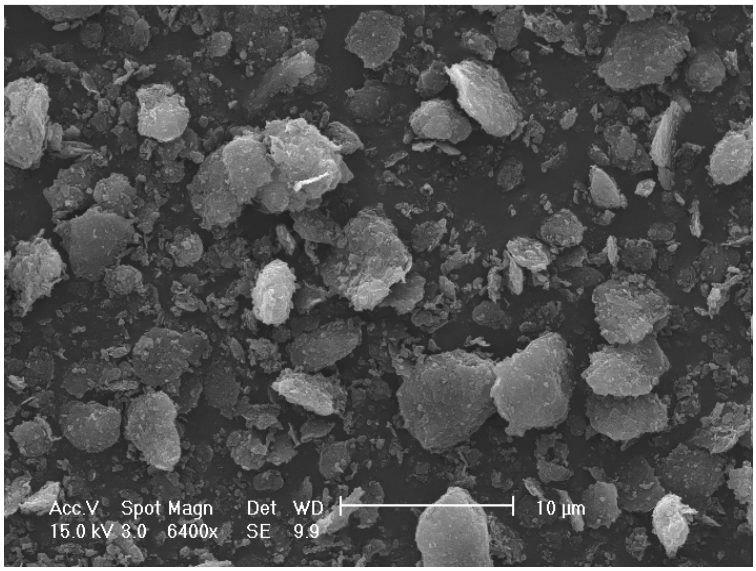

Fig.A. Graphite powder SEM image

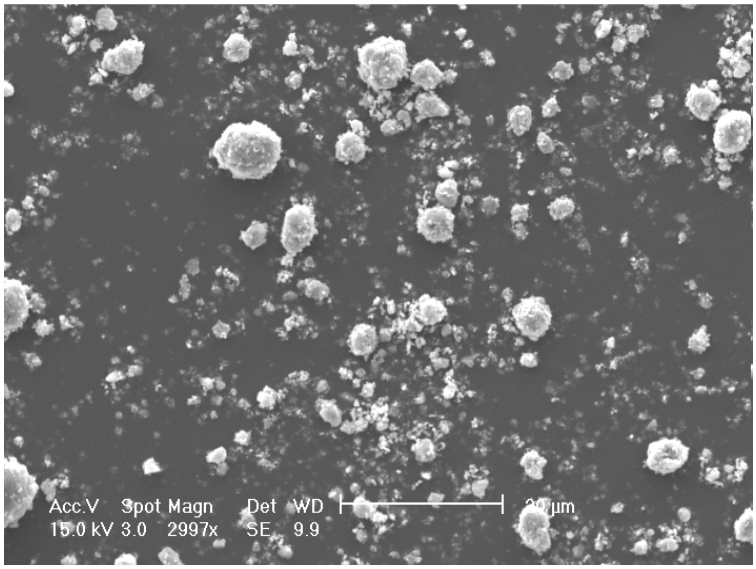

Fig.B. Nickel powder SEM image

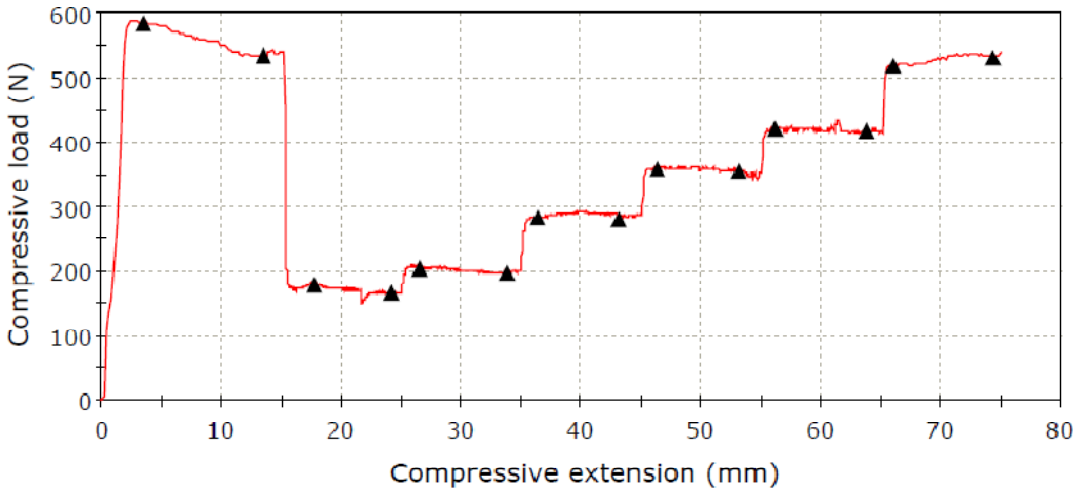

Fig.C. Play-doh Load vs. Extension for L/D 1

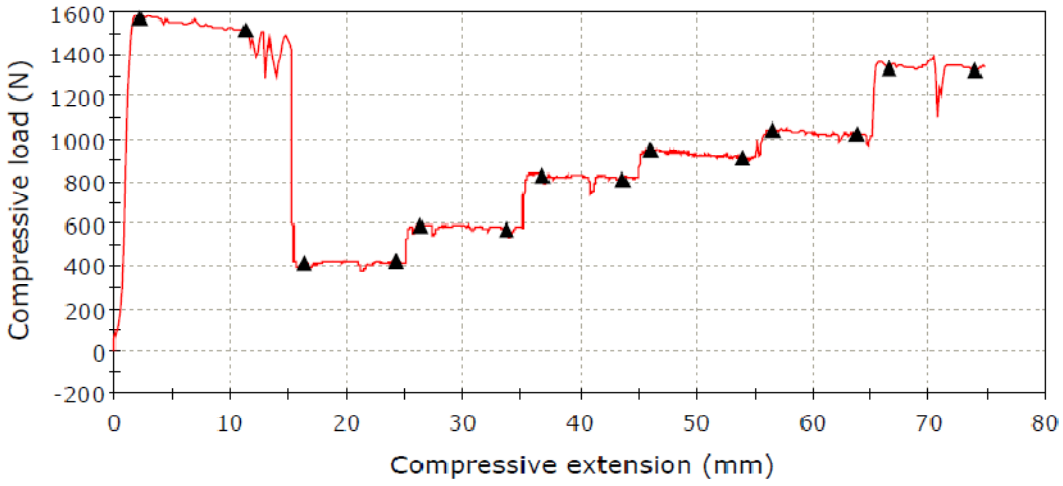

Fig.D. Play –doh Load vs. Extension for L/D 8

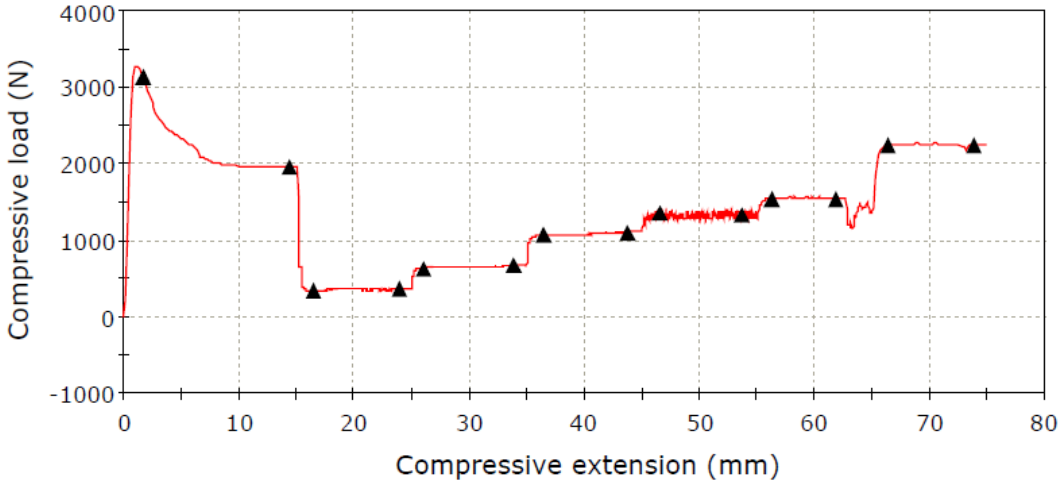

Fig.E. Play-doh Load vs. Extension for L/D 16